NASA TECHNICAL MEMORANDUM

NASA TM X-3537

NASA TM X-3537

INLET REYNOLDS NUMBER AND TEMPERATURE EFFECTS ON THE STEADY-STATE PERFORMANCE OF A TFE731-2 TURBOFAN ENGINE

George A. Bobula and Roy A. Lottig

Lewis Research Center
and
Lewis Directorate,
U.S. Army Air Mobility R&D Laboratory
Cleveland, Ohio 44135

NATIONAL AERONAUTICS AND SPACE ADMINISTRATION · WASHINGTON, D. C. · MAY 1977

1. Report No. NASA TM X-3537	2. Government Accession No.	3. Recipient's Catalog No.
4. Title and Subtitle INLET REYNOLDS NUMBER AND TEMPERATURE EFFECTS ON THE STEADY-STATE PERFORMANCE OF A TFE731-2 TURBOFAN ENGINE		5. Report Date May 1977
		6. Performing Organization Code
7. Author(s) George A. Bobula and Roy A. Lottig		8. Performing Organization Report No. E-8941
		10. Work Unit No. 505-05
9. Performing Organization Name and Address NASA Lewis Research Center and U.S. Army Air Mobility R&D Laboratory Cleveland, Ohio 44135		11. Contract or Grant No.
		13. Type of Report and Period Covered Technical Memorandum
12. Sponsoring Agency Name and Address National Aeronautics and Space Administration Washington, D.C. 20546		14. Sponsoring Agency Code

15. Supplementary Notes

16. Abstract

Effects of varying engine inlet Reynolds number index (0.75, 0.50, 0.25, and 0.12) and temperature (289 and 244 K) on a TFE731-2 turbofan engine were evaluated. Results were classified as either compression system effects or effects on overall performance. Standard performance maps are used to present compression system performance. Overall performance parameters are presented as a function of low rotor speed corrected to engine inlet temperature.

17. Key Words (Suggested by Author(s)) Turbofan engine; Reynolds number effects; Temperature effects; Steady-state performance	18. Distribution Statement Unclassified - unlimited STAR Category 07		
19. Security Classif. (of this report) Unclassified	20. Security Classif. (of this page) Unclassified	21. No. of Pages 49	22. Price* A03

* For sale by the National Technical Information Service, Springfield, Virginia 22161

INLET REYNOLDS NUMBER AND TEMPERATURE EFFECTS ON

THE STEADY-STATE PERFORMANCE OF A

TFE731-2 TURBOFAN ENGINE

by George A. Bobula and Roy A. Lottig

Lewis Research Center and
U. S. Army Air Mobility R&D Laboratory

SUMMARY

An experimental investigation to determine the effects of engine inlet Reynolds number and temperature on a moderately high bypass ratio turbofan engine, the TFE731-2, was conducted at the Lewis Research Center. Tests were conducted at a constant Mach number of 0.8, engine inlet Reynolds number indices of 0.75, 0.50, 0.25, and 0.12, and inlet temperatures of 289 and 244 K.

Decreased engine inlet Reynolds number resulted in decreased corrected engine airflows and compression efficiencies, and increased bypass ratio, compression system temperature ratio, interturbine temperature ratio, turbine exit temperature ratio, and corrected fuel flow. Decreased engine inlet temperature resulted in decreased corrected engine airflow, fan hub efficiency and corrected fuel flow, and increased compression temperature ratio, turbine exit temperature ratio, and interturbine temperature ratio. Speed match was affected by Reynolds number only at the 244 K inlet temperature where a reversal in trend occurred.

INTRODUCTION

An experimental investigation was performed to determine the effects of engine inlet Reynolds number and temperature on the steady-state performance of a TFE731-2 turbofan engine. Variations of engine inlet Reynolds number and temperature which occur with changes in aircraft flight condition affect gas turbine engine performance. Such effects on turbojet and turbofan engines are documented, for example, in references 1 to 9. The literature concerned with these effects on turbofan engines is more limited,

however. An investigation into the engine inlet Reynolds number and temperature effects on the TFE731-2 engine, which has several unique design features, can therefore contribute to the understanding of turbofan engine performance.

The engine reported herein is a moderately high bypass ratio, two spool gas turbine with a geared front fan. It has an axial low pressure compressor, a centrifugal high pressure compressor, and a reverse flow annular combustor.

Tests were performed at a simulated Mach number of 0.8, over a range of engine inlet Reynolds number index from 0.12 to 0.75, and at engine inlet temperatures of 289 and 244 K (520° and 440° R). Reynolds number index is defined as the ratio of the local Reynolds number at the flight condition to that at standard sea-level conditions.

APPARATUS AND PROCEDURE

Engine

The AiResearch Model TFE731-2 (serial number 7306 Build No. 2) turbofan engine tested in this program is a 15 600-newton (3500-lb) thrust, moderately high bypass ratio, two spool gas turbine with a geared front fan. The 0.556 gear reduction design also results in the fan rotating counter to the low pressure compressor. The single-stage fan and four-stage axial low pressure compressor are driven by a three-stage axial turbine. The single-stage centrifugal high pressure compressor discharges into a reverse flow, annular combustor. The high spool is driven by a single-stage axial turbine which also drives the accessory gearbox. Fan and core flows discharge through coannular separated flow nozzles of areas 1262 and 617 cm^2 (195.6 and 95.6 in.^{2}), respectively. Figure 1(a) is a schematic diagram depicting the airflow paths. Reference 10 presents further details of the engine design.

Instrumentation

The instrumentation configuration for data reported in this text is shown in figure 1. Engine inlet temperature was measured upstream of the bellmouth at station 1. Total engine airflow was based on the temperature measured at station 1.0 and a pressure survey at station 1.2. The majority of the instrumentation divided the compression system into fan tip (stations 2 to 9), fan hub (2 to 22), low pressure compressor (22 to 24), and high pressure compressor (24 to 3). The remaining probes were placed to evaluate overall engine performance (stations 5, 7, 8, 11, and 12).

Pressure, temperature, speeds, and other reported parameters were recorded on the Lewis Central Automatic Digital Data Encoder (CADDE) (ref. 11).

Engine Installation

The engine installation in the altitude test chamber is shown in figure 2. The installation was of a conventional direct-connect type, with the inlet bellmouth located in a plenum upstream of the engine chamber. The plenum was isolated from the test chamber by the front bulkhead (fig. 2(b)). Conditioned air was supplied to the inlet plenum to yield the desired engine inlet Reynolds number index and temperature. The air consumed by the engine was discharged through the exhaust nozzles and, with any test cell cooling air, passed into the exhaust collector (fig. 2(c)). The test chamber altitude pressure was controlled by valves downstream of the installation.

Test Procedure

During these tests, a constant ram pressure ratio $P_{T,2}/P_{ALT}$ of 1.525, corresponding to a simulated Mach number M_0 of 0.8, was maintained. (Symbols are defined in appendix A.) Testing was conducted at engine inlet total temperatures of 289 and 244 K (520° and 440° R). At a given inlet temperature, inlet pressure was adjusted to achieve the desired engine inlet Reynolds number index while altitude pressure was adjusted to maintain ram pressure ratio.

Operating line data were obtained at the following combinations of inlet temperature $T_{T,2}$ and Reynolds number index RNI_2: $T_{T,2}$ = 289 K, RNI_2 = 0.75, 0.50, 0.25; $T_{T,2}$ = 244 K, RNI_2 = 0.50, 0.25, 0.12. The possibility of an effect of inlet temperature was thus evaluated at RNI_2 values of 0.50 and 0.25. The 244 K $T_{T,2}$ also permitted acquisition of limited data at 0.12 RNI_2 and of the higher corrected speed data for 0.50 and 0.25 RNI_2 without encountering turbine temperature limits.

RESULTS AND DISCUSSION

The first section of results presents the engine inlet Reynolds number index and temperature effects on the fan, low pressure compressor, and high pressure compressor performance. These results are followed by the engine inlet Reynolds number index and temperature effects on some of the engine performance parameters. All data presented were referred to the highest power setting tested at the 0.75 RNI_2 condition.

Component Performance

Fan performance. - The fan tip and fan hub performance maps are presented in

3

figure 3. The open symbols represent the 289 K $T_{T,2}$ data and the shaded symbols represent the 244 K $T_{T,2}$ data.

The data of figures 3(a) and (b) show that the fan tip and hub pressure ratios were independent of RNI_2 and $T_{T,2}$ at a given corrected speed until RNI_2 reached 0.12. At 0.12 RNI_2, the fan tip pressure ratio fell 1.5 percent below the higher RNI_2 data at 95 percent reference fan speed.

The data of figures 3(c) and (d) show that for a given fan tip or fan hub pressure ratio, corrected airflow decreased as RNI_2 decreased. The data indicate no significant $T_{T,2}$ effect at 0.50 RNI_2; while at 0.25 RNI_2, the 244 K data was 1 to 1.5 percent lower in airflow than the 289 K data. The same trend in corrected airflow occurred with RNI_2 and $T_{T,2}$ at a given corrected speed (fig. 3(e)).

Fan tip and fan hub efficiencies (figs. 3(f) and (g)) generally decreased with decreasing RNI_2. Fan hub efficiency also decreased with decreasing $T_{T,2}$. The majority of the data indicated that near 103 percent of the reference corrected speed, all but the 0.12 RNI_2 fan tip efficiency data approached a value near 100 percent of the reference fan tip efficiency. The lower fan tip efficiency at 0.12 RNI_2 accompanied the drop in pressure ratio previously noted. The fan hub efficiency data showed a merging at higher corrected speeds, but the trend was not quite as strong in this case. Because of the general drop in efficiency as RNI_2 and $T_{T,2}$ were lowered, it is to be expected that more turbine work would be necessary to maintain a given speed. This will be displayed later in the text.

Low pressure axial flow compressor performance. - Low pressure compressor LPC performance is presented in figure 4. The data of figure 4(a), the LPC pressure ratio-corrected speed relationship, showed no dependence on either RNI_2 or $T_{T,2}$. In figures 4(b) and (c), corrected airflow dropped as RNI_2 decreased either at a given pressure ratio or corrected speed, as previously noted in the fan. There was no effect of $T_{T,2}$ on LPC airflow.

The major variation of LPC efficiency, shown in figure 4(d), occurred between 0.50 RNI_2 and 0.25 RNI_2, the lower RNI_2 data falling 2 to 2.5 percent below the higher RNI_2 data up to 100 percent reference corrected speed. Near 105 percent speed, the efficiencies were equal.

High pressure centrifugal compressor performance. - The high pressure compressor HPC performance is presented in figure 5. Once again, the pressure ratio-corrected speed relationship (fig. 5(a)) was independent of RNI_2 and $T_{T,2}$. Decreased RNI_2 at a given pressure ratio or corrected speed resulted in decreased corrected airflow (figs. 5(b) and (c)). No effect of $T_{T,2}$ on corrected airflow was noted.

HPC efficiency plotted against corrected speed (fig. 5(d)) showed that lower RNI_2 yielded lower efficiency above 97 percent reference corrected speed for the data available. Instrumentation problems prevented determination of HPC efficiency at

0.12 RNI_2 and at 0.25 RNI_2 with a $T_{T,2}$ of 289 K. There was no effect of $T_{T,2}$ on efficiency.

The presentation of inlet Reynolds number index and temperature effects on the individual compression system components has indicated primarily a drop in both corrected airflow and efficiency as RNI_2 was reduced. Only the fan was affected by $T_{T,2}$ variation, these secondary effects being a further drop in total corrected airflow and an additional decrease in fan hub efficiency as $T_{T,2}$ decreased.

All components but the fan tip showed pressure ratio independent of RNI_2. At 0.12 RNI_2, the fan tip pressure ratio fell below the higher RNI_2 data.

Effects on Engine Performance

The low rotor speed corrected to engine inlet temperature was chosen as the independent variable against which engine performance parameters would be plotted. This choice was made because the low rotor is related to both fan and core performance. Data comparisons will be made at a corrected low rotor speed of 95 percent of reference, unless it is noted otherwise. A tabulation is made of the comparison data in table I.

Compression system overall performance. - Figure 6 presents the overall performance of the compression system. Since low rotor speed and fan speed are related by a constant, normalized corrected fan speed is equal to normalized corrected low rotor speed. Therefore, figure 6(a) is identical to figure 3(e). Figure 6(a) is shown to complete the presentation. The figures show that decreasing RNI_2 from 0.75 to 0.50 at 289 K $T_{T,2}$ decreased airflow by 0.5 percent. A further decrease in RNI_2 to 0.25 yielded a further drop in airflow of 0.7 percent. $T_{T,2}$ had essentially no effect at 0.50 RNI_2, while at 0.25 RNI_2, the 244 K data was 1.5 percent lower in airflow than the 289 K data. Part of this change in airflow may be due to changes in the engine match with $T_{T,2}$ changes.

The core compression system overall pressure ratio $P_{T,3}/P_{T,2}$ (fig. 6(b)) was essentially independent of both RNI_2 and $T_{T,2}$ throughout the range of corrected low rotor speed tested. However, with fan and compressor efficiencies dependent on engine inlet conditions, figure 6(c) shows the resulting effect on core compression system total temperature ratio. As RNI_2 was decreased from 0.75 to 0.50, $T_{T,3}/T_{T,2}$ increased 0.5 percent. Decreasing RNI_2 further to 0.25 resulted in an additional rise in temperature ratio of 1.0 percent at 289 K $T_{T,2}$. At 244 K $T_{T,2}$, the increase was 2.2 percent between 0.25 and 0.12 RNI_2. It was also noted that the 244 K $T_{T,2}$ data at 0.50 and 0.25 RNI_2 were 1.2 percent and 0.9 percent higher in $T_{T,3}/T_{T,2}$ than the respective data at 289 K $T_{T,2}$.

Energy requirements. - Figure 7 shows the effects of RNI_2 and $T_{T,2}$ on the energy requirements within the engine. The lower compression efficiencies that

resulted with decreased RNI_2 should require increased turbine work to operate the engine at the same corrected low rotor speed. Energy input to the engine, as reflected in corrected fuel flow (fig. 7(a)), increased 3.2 percent as RNI_2 decreased from 0.75 to 0.50 and interturbine temperature ratio (fig. 7(b)), $T_{T,5}/T_{T,2}$, increased 1.6 percent, indicating an increased turbine energy level was required to maintain 95 percent corrected low rotor speed.

Corrected fuel flow and interturbine temperature ratio also showed the effects of inlet temperature variation. Corrected fuel flow decreased 3.2 percent at 0.5 RNI_2 and 6.2 percent at 0.25 RNI_2 as $T_{T,2}$ was decreased from 289 to 244 K. Interturbine temperature ratio increased 1.2 percent and 3 percent for the same $T_{T,2}$ changes. Aside from possible engine match changes previously mentioned, specific heat and specific heat ratio variations with temperature through the engine are believed to be a contributing factor to these effects. The parameters used to refer speeds, fuel flows, airflows, and temperatures to standard conditions are derived from dimensional analysis and assume negligible specific heat effects. By basing correction parameters on dynamic similarity, specific heat variations can be accounted for (refs. 12 and 13). In a report on this engine (ref. 14) the authors suggested modified correction parameters, both theoretically and empirically determined. These parameters, while offering a better correlation of data at the same RNI_2 but different $T_{T,2}$ values, did not bring about total agreement. With the limited inlet temperature variation of this test, new modified correction parameters were not evaluated. It was only determined that there was an effect of inlet temperature on some parameters.

Overall cycle performance. - Figure 8 presents the effects of engine inlet conditions on overall cycle pressure and temperature ratios. In figures 8(a) and (b) fan duct total pressure ratio $P_{T,11}/P_{T,2}$ and engine pressure ratio $P_{T,7}/P_{T,2}$ are seen to be independent of RNI_2 and $T_{T,2}$. The fan duct total temperature ratio (fig. 8(c)) was essentially independent of RNI_2 and $T_{T,2}$. Only the 0.12 RNI_2 data appeared to differ, being at most 0.5 percent higher than the rest of the data. The core engine total temperature ratio (fig. 8(d)) showed the result of operating at a constant corrected low rotor speed, and therefore constant cycle pressure ratio, while decreasing RNI_2. The decreasing component efficiencies and increasing heat addition, resulting in entropy increases, yielded a higher final enthalpy state. Thus, as RNI_2 decreased from 0.75 to 0.50, turbine exit temperature ratio $T_{T,7}/T_{T,2}$ rose 1.7 percent. Decreasing RNI_2 further to 0.25 yielded an additional $T_{T,7}/T_{T,2}$ rise of 4.3 percent. The lower temperature data showed similar trends.

The only parameter in figure 8 showing an effect of $T_{T,2}$ was $T_{T,7}/T_{T,2}$. Decreasing $T_{T,2}$ from 289 to 244 K at 0.50 RNI_2 yielded negligible change; while at 0.25 RNI_2, the ratio increased 1.9 percent.

Core and fan stream matching. - The match between core and fan streams is evaluated using bypass ratio (BPR) and also the speed match. Bypass ratio is the ratio of

the airflow bypassed through the fan duct to the airflow entering the engine core. The core inlet airflow was determined from core exhaust gas flow, fuel flow, and cooling flows. The core exhaust gas flow was based on measurements of exhaust gas condition and nozzle model calibration test results. The model tests were performed by the engine manufacturer and verified during the altitude-performance testing of reference 14. Fan duct airflow was calculated as total engine airflow minus core inlet airflow.

Nozzle total-to-static pressure ratios are the forcing functions of core and fan nozzle corrected flows. Since the tests were performed at a constant $P_{T,2}/P_{ALT}$, the variation of exhaust nozzle total-to-static pressure ratio was implied in figures 8(a) and (b), the cycle total pressure ratios, for example,

$$\frac{P_{T,11}}{P_{ALT}} = \left(\frac{P_{T,11}}{P_{T,2}}\right)\left(\frac{P_{T,2}}{P_{ALT}}\right)$$

There is, however, another effect not associated with engine inlet conditions revealed in figure 9(a). Here it is seen that, over the engine operating range, the fan nozzle exit external static pressure agrees with ambient pressure. The core nozzle exit external static pressure, however, is seen to increase with power setting due to the effect of the fan flow field on the core stream. The resulting nozzle total-to-static pressure ratios are shown in figures 9(b) and (c). All nozzle performance figures showed no dependence on engine inlet conditions.

At the test ram pressure ratio of 1.525, the exhaust nozzles were unchoked over much of the engine operating range. The choked flow regions indicated in the figures were determined from the nozzle calibration tests. Although the fan nozzle operated at a higher pressure ratio than the core nozzle at the lower speeds and choked before the core, figure 9(c) shows that the core nozzle pressure ratio increased approximately twice as fast as that of the fan. The core nozzle choked soon after the fan. The resulting corrected core nozzle gas flow, presented in figure 9(d), is independent of engine inlet conditions.

Bypass ratio, as seen in figure 10(a), can be expressed as

$$BPR = \frac{WA_9}{WA_{22}}$$

or, by rearranging as in appendix B, BPR can be represented solely in terms of parameters presented in previous figures as

$$BPR = \cfrac{\left(\cfrac{WA_2 \sqrt{\theta_2}}{\delta_2}\right)}{K\left[\cfrac{\left(\cfrac{WG_7 \sqrt{\theta_7}}{\delta_7}\right)(EPR)}{\sqrt{\cfrac{T_{T,7}}{T_{T,2}}}} - \left(\cfrac{WF}{\sqrt{\theta_2}\,\delta_2}\right)(\theta_2)\right]} - 1$$

Bypass ratio increased 1.3 percent as RNI_2 decreased from 0.75 to 0.50 and 2.1 percent as RNI_2 decreased from 0.50 to 0.25. Examination of the behavior of the various parameters in the second representation for BPR revealed that only $T_{T,7}/T_{T,2}$ and $WF/(\sqrt{\theta_2}\,\delta_2)$ were affected in such a way by decreasing RNI_2 so as to yield an increase in BPR. Examining the relative magnitudes of the effect of these parameters on BPR showed that the BPR increase was due mainly to increased $T_{T,7}/T_{T,2}$.

The speed match of figure 10(b) shows no dependence on RNI_2 at 289 K $T_{T,2}$. At 244 K $T_{T,2}$, however, effects of RNI_2 were seen. The 244 K $T_{T,2}$ data at 0.50 RNI_2 was 1.3 percent higher in corrected high rotor speed than the 289 K data. The cold 0.25 RNI_2 data fell 0.5 percent below the cold 0.50 RNI_2 data, while the 0.12 RNI_2 data was 0.9 percent above that at 0.50 RNI_2. This reversal is believed to be genuine as data recorded at a later date repeated the trend.

It is believed that the speed match trends were due to turbine performance and matching changes. Sufficient turbine instrumentation was not available to verify this, however.

SUMMARY OF RESULTS

An investigation was undertaken to determine the effects of engine inlet Reynolds number and temperature on the fan, compressor, and overall engine performance of a TFE731-2 turbofan engine. Inlet Reynolds number indices of 0.75, 0.50, 0.25, and 0.12 were examined at inlet temperatures of 289 and 244 K (520° and 440° R), at a ram pressure ratio of 1.525. The summarized results are as follows:

1. A reduction of inlet Reynolds number index RNI_2 resulted in decreased fan and compressor corrected airflow and efficiency at a given corrected speed.

2. Fan and compressor total pressure ratios were independent of RNI_2 to values of 0.25; and at 0.12 RNI_2, only fan tip pressure ratio suffered a loss.

3. Fan airflow decreased with decreasing inlet total temperature $T_{T,2}$, the effect being more noticeable at 0.25 RNI_2.

4. Fan hub efficiency decreased with decreasing $T_{T,2}$.

5. The compressor operating lines were unaffected by $T_{T,2}$.

6. The overall fan/compressor total pressure ratio, engine pressure ratio, and fan duct total pressure ratio were essentially independent of RNI_2 and $T_{T,2}$ at a given corrected low rotor speed.

7. Overall core compression system temperature ratio, interturbine temperature ratio, turbine exit temperature ratio, and corrected fuel flow increased as RNI_2 decreased at a fixed corrected low rotor speed.

8. Decreased engine inlet temperature resulted in increased core compression system temperature ratio, interturbine temperature ratio and turbine exit temperature ratio, and a decreased corrected fuel flow at a given corrected low rotor speed.

9. Bypass ratio increased as RNI_2 decreased but was independent of $T_{T,2}$.

10. Speed match was independent of RNI_2 at 289 K $T_{T,2}$. At 244 K $T_{T,2}$, decreasing RNI_2 showed an initial drop in corrected high rotor speed, followed by a reversal and increase in high rotor speed as RNI_2 continued to drop.

Lewis Research Center,

    National Aeronautics and Space Administration,

        and

U.S. Army Air Mobility R&D Laboratory,

    Cleveland, Ohio, November 19, 1976,

        505-05.

APPENDIX A

SYMBOLS

BPR   bypass ratio (e.g., ratio of fan duct airflow at fan tip discharge to core engine airflow at fan hub discharge)

EPR   engine pressure ratio (e.g., ratio of turbine exit total pressure to engine inlet total pressure)

M_0 simulated Mach number

NF   fan speed, 0.556 NL, rpm

NH   high rotor speed, rpm

NL   low rotor speed, rpm

P_S static pressure, N/cm^2

P_T total pressure, N/cm^2

RNI   Reynolds number index, $\delta/(\varphi\sqrt{\theta})$

T_T total temperature, K

WA   air flow rate, kg/sec

WF   fuel flow rate, kg/hr

WG   gas flow rate, kg/hr

δ ratio of total pressure to absolute pressure of NASA standard sea-level conditions

η adiabatic efficiency

θ ratio of total temperature to absolute temperature of NASA standard sea-level conditions

φ ratio of viscosity to viscosity of NASA standard sea-level conditions

Subscripts:

ALT   simulated altitude

FH   fan hub

FT   fan tip

HPC   high pressure compressor

LPC   low pressure compressor

ref   reference condition

2   fan inlet

3   HPC discharge

5   interurbine

7   turbine discharge

8   core nozzle discharge

9   fan tip discharge

11 fan nozzle inlet

12 fan nozzle discharge

22 fan hub exit and LPC inlet

24 LPC discharge and HPC inlet

APPENDIX B

BYPASS RATIO DEPENDENCY

While bypass ratio BPR was defined for this report as WA_9/WA_{22}, its calculation was somewhat more involved. The calculations are detailed below:

$$BPR = \frac{WA_9}{WA_{22}}$$

$$WA_9 = WA_2 - WA_{22}$$

where WA_2 was based on an airflow survey at station 1.2 and WA_{22} was based on core exhaust nozzle calibration information, fuel flow, and bleed flows.

The dependence of BPR on other parameters reported herein may be further developed as follows:

$$BPR = \frac{WA_9}{WA_{22}} = \frac{WA_2 - WA_{22}}{WA_{22}} = \frac{WA_2}{WA_{22}} - 1$$

$$1 + BPR = \frac{WA_2}{WA_{22}}$$

$$WA_{22} = K(WA_7) = K(WG_7 - WF)$$

where K is an empirically determined constant accounting for bleed flows. Thus,

$$1 + BPR = \frac{WA_2}{WA_{22}} = \frac{\dfrac{WA_2 \sqrt{\theta_2}}{\delta_2}}{K \dfrac{\sqrt{\theta_2}}{\delta_2}(WG_7 - WF)} = \frac{\dfrac{WA_2 \sqrt{\theta_2}}{\delta_2}}{K\left[\left(\dfrac{WG_7 \sqrt{\theta_7}}{\delta_7}\right)\left(\dfrac{\delta_7}{\delta_2}\right)\left(\sqrt{\dfrac{\theta_2}{\theta_7}}\right) - \left(\dfrac{WF}{\sqrt{\theta_2}\,\delta_2}\right)(\theta_2)\right]}$$

$$1 + \mathrm{BPR} = \cfrac{\dfrac{\mathrm{WA}_2 \sqrt{\theta_2}}{\delta_2}}{\mathrm{K}\left[\cfrac{\left(\dfrac{\mathrm{WG}_7 \sqrt{\theta_7}}{\delta_7}\right)(\mathrm{EPR})}{\sqrt{\dfrac{\mathrm{T}_{\mathrm{T},7}}{\mathrm{T}_{\mathrm{T},2}}}} - \left(\dfrac{\mathrm{WF}}{\sqrt{\theta_2}\,\delta_2}\right)(\theta_2)\right]}$$

REFERENCES

1. Benser, W. A.; Finger, H. B.: Compressor-Stall Problems in Gas-Turbine Type Aircraft Engines. SAE Paper 751, Apr. 1956.

2. Campbell, Carl E.; and Sobolewski, Adam E.: Altitude-Chamber Investigation of J73-GE-1A Turbojet Engine Component Performance. NACA RM E53I08, 1954.

3. Wallner, Lewis E.; and Fleming, William A.: Reynolds Number Effect on Axial-Flow Compressor Performance. NACA RM E9G11, 1949.

4. NACA Conference on Aircraft Propulsion Systems Research. NACA, 1950.

5. Sanders, Newell D.; and Behun, Michael: Generalization of Turbojet-Engine Performance in Terms of Pumping Characteristics. NACA TN 1927, 1949.

6. Walker, Curtis L.; Huntley, S. C.; and Braithwaite, W. M.: Component and Over-All Performance Evaluation of an Axial-Flow Turbojet Engine Over a Range of Engine-Inlet Reynolds Numbers. NACA RM E52B08, 1952.

7. Seashore, Ferris L.; and Corrington, Lester C.: Component Performance of J71-A-2 (600-D1) Turbojet Engine at Several Reynolds Number Indices. NACA RM E56B14, 1956.

8. Campbell, Carl E.: Performance of Basic XJ79-GE-1 Turbojet Engine and Its Components. NACA RM E58C12, 1958.

9. Biesiadny, Thomas J.; Grey, Rudolph E.; and Abdelwahab, Mahmood: Altitude Performance of a Low-Noise-Technology Fan in a Turbofan Engine With and Without a Sound Suppressing Nacelle. NASA TM X-3385, 1976.

10. Steele, M. C.; and Roberts, F. L.: Highlights of the Design and Development of a Modern Geared-Fan Jet Engine. SAE Paper 720351, Mar. 1972.

11. Central Automatic Data Processing System. NACA TN 4212, 1958.

12. Glassman, Arthur J., ed.: Basic Turbine Concepts. Turbine Design and Application. NASA SP-290, Vol. 1, 1972, pp. 21-68.

13. Lancaster, O. E., ed.: Jet Propulsion Engines. Vol. XII, Princeton Univ. Press, 1959.

14. Dixon, G. J.; Davenport, W. R.; and Steele, M. A.: Engineering Test Report of Altitude - Performance Test Conducted at NASA Lewis Research Center on Airesearch Model TFE 731-2 Turbofan Engine. PE-8296-R, AiResearch Mfg. Co., 1972.

TABLE I. - CHANGES IN ENGINE PERFORMANCE
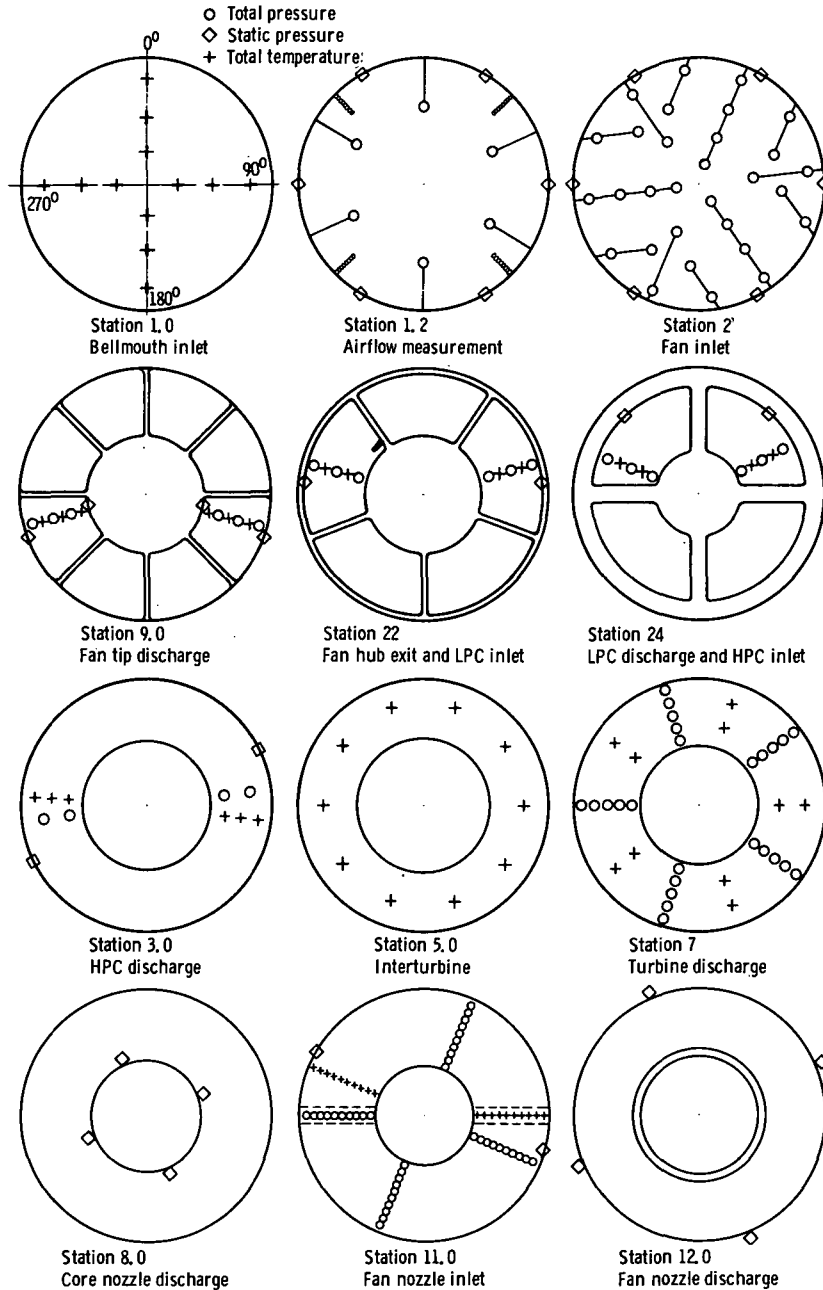
PARAMETERS FROM VALUE AT $RNI_2 = 0.75$

AND $NL/\sqrt{\theta_2} = 95$ PERCENT $(NL/\sqrt{\theta_2})_{ref}$

[+ indicates increases; - indicates decreases.]

Parameter	Inlet Reynolds number index, RNI_2				
	0.50		0.25		0.12
	Inlet total temperature, $T_{T,2}$, K				
	289	244	289	244	244
$WA_2\sqrt{\theta_2}/\delta_2$	-0.5	-0.5	-1.2	-2.7	-5.2
$T_{T,3}/T_{T,2}$	+.5	+1.7	+1.5	+2.4	+4.6
$WF/(\sqrt{\theta_2}\,\delta_2)$	+3.2	0	+6.2	0	+6.2
$T_{T,5}/T_{T,2}$	+1.6	+2.8	+4.7	+7.7	+15.7
$T_{T,11}/T_{T,2}$	0	0	0	0	+.5
$T_{T,7}/T_{T,2}$	+1.7	+1.7	+6.0	+7.9	+18.3
BPR	+1.3	+1.3	+3.4	+3.4	+5.5
$NH/\sqrt{\theta_2}$	0	+1.3	0	+.8	+2.2
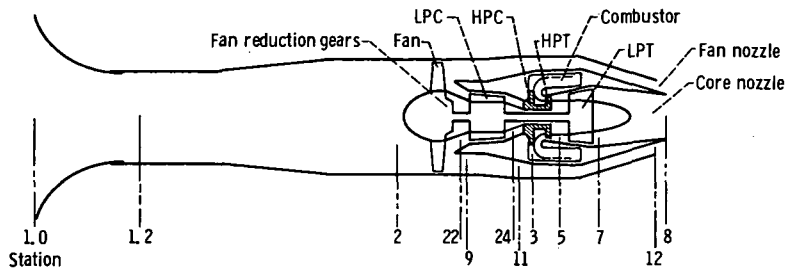
(a) Station locations and flowpath.

- ○ Total pressure
- ◇ Static pressure
- + Total temperature

Station 1.0
Bellmouth inlet

Station 1.2
Airflow measurement

Station 2
Fan inlet

Station 9.0
Fan tip discharge

Station 22
Fan hub exit and LPC inlet

Station 24
LPC discharge and HPC inlet

Station 3.0
HPC discharge

Station 5.0
Interturbine

Station 7
Turbine discharge

Station 8.0
Core nozzle discharge

Station 11.0
Fan nozzle inlet

Station 12.0
Fan nozzle discharge

(b) Individual station layouts (looking upstream).

CD-12065-07

Figure 1. - Schematic of TFE731-2 engine and instrumentation.
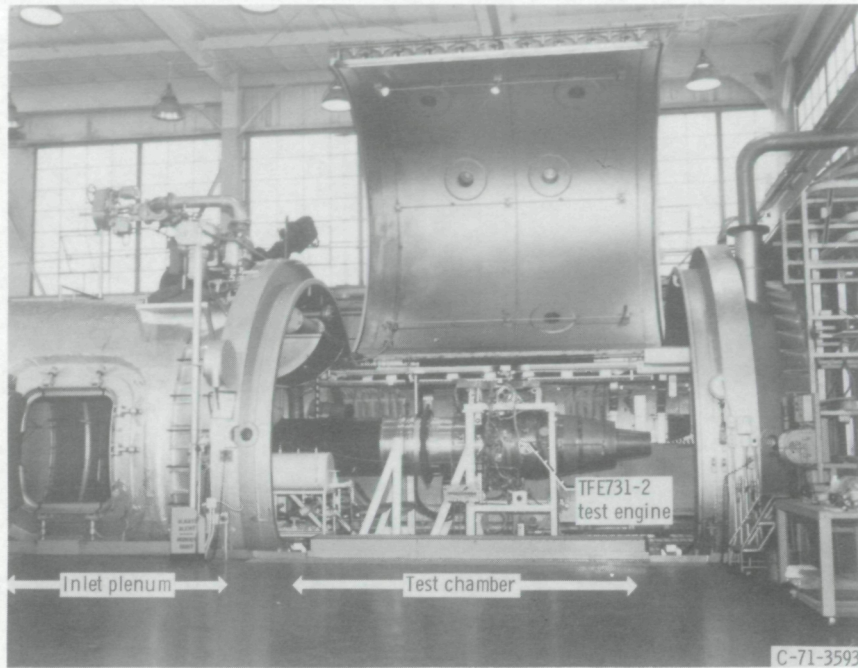
(a) Installation in altitude facility.
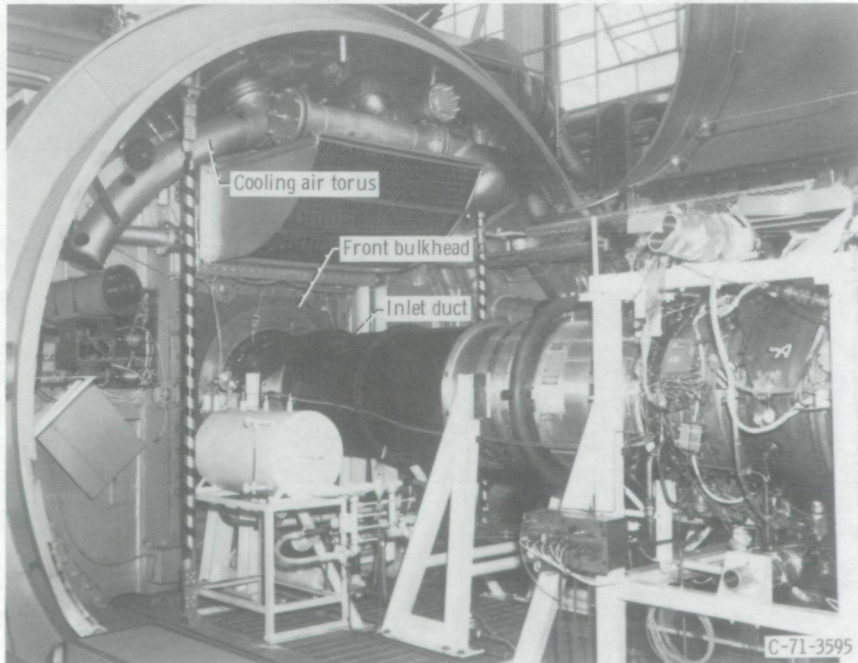
(b) Front bulkhead and inlet ducting.
Figure 2. – Engine installation.

17
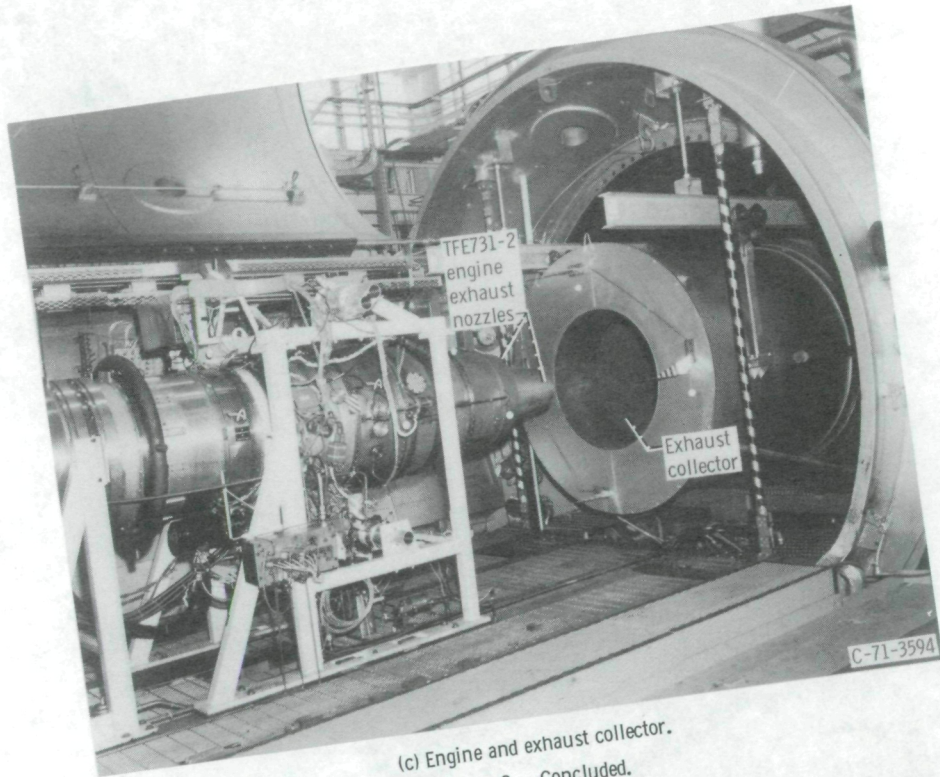
(c) Engine and exhaust collector.

Figure 2. - Concluded.

Percent of reference fan tip pressure ratio, percent $(P_{t,9}/P_{t,2})_{ref}$

Inlet Reynolds number index, RNI_2

0.75
.50
.25
.12

○ □ △ ◇

Open symbols denote 289 K inlet total temperature
Shaded symbols denote 244 K inlet total temperature

Percent of reference corrected fan speed, percent $(NF/\sqrt{\theta_2})_{ref}$
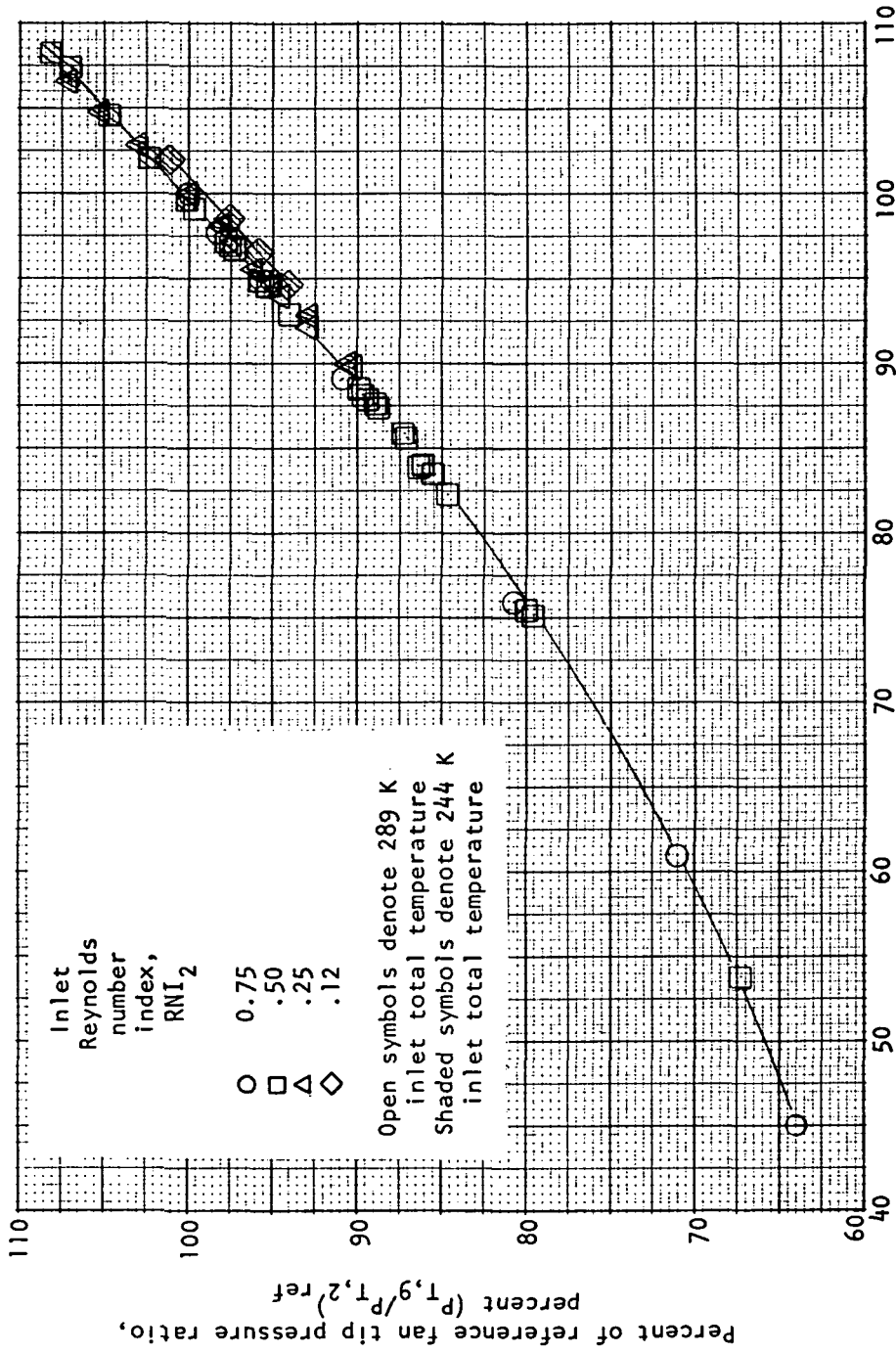
(a) Fan tip pressure ratio plotted against corrected fan speed.

Figure 3. – Fan performance at simulated Mach number $M_0 = 0.8$.
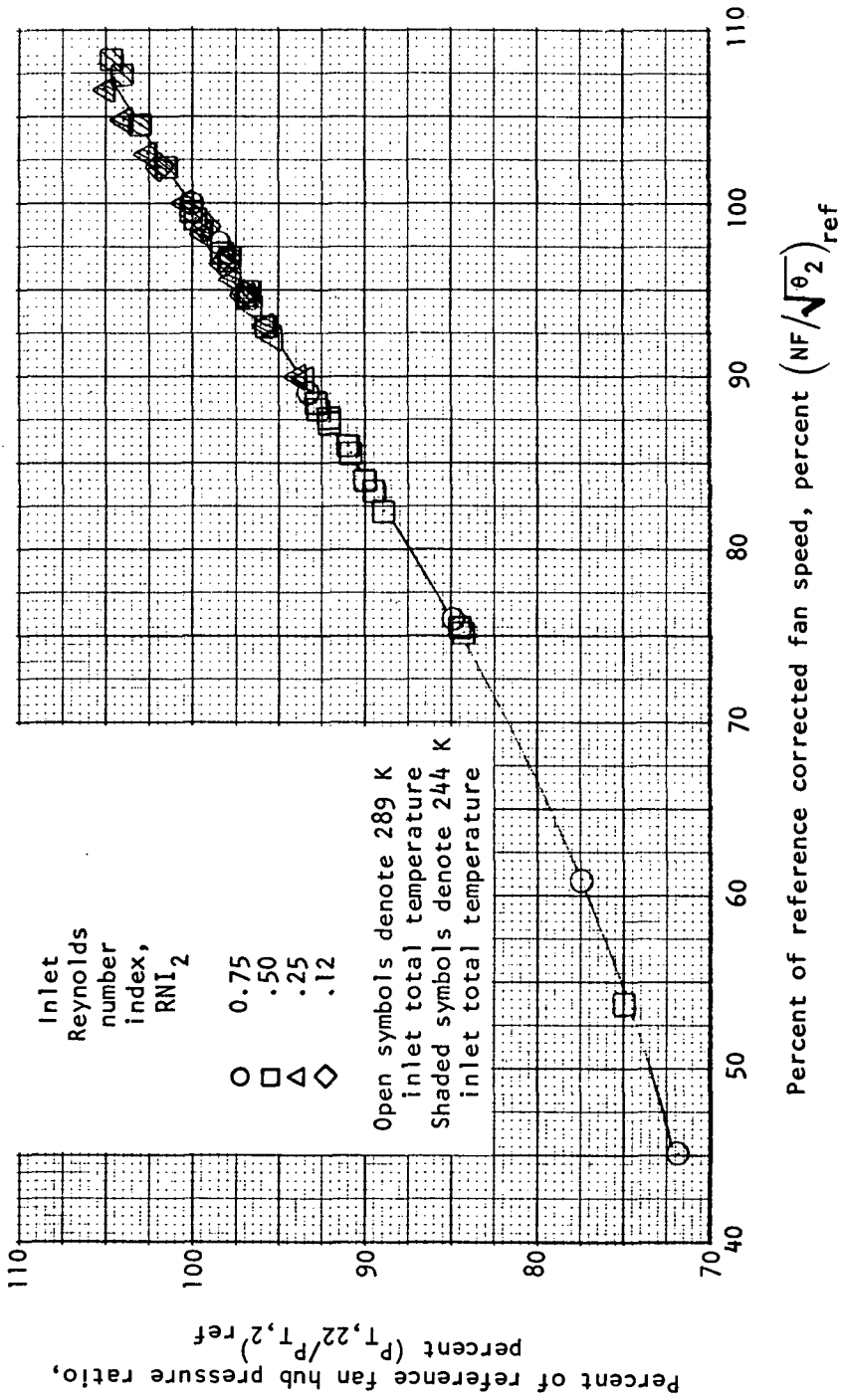
(b) Fan hub pressure ratio plotted against corrected fan speed.

Figure 3. – Continued.

Inlet Reynolds number index, RNI_2

○ 0.75
□ .50
◁ .25
◇ .12

Open symbols denote 289 K inlet total temperature
Shaded symbols denote 244 K inlet total temperature

Percent of reference corrected fan speed, percent $\left(NF/\sqrt{\theta_2}\right)_{ref}$

Percent of reference fan hub pressure ratio, percent $\left(P_{T,22}/P_{T,2}\right)_{ref}$

20
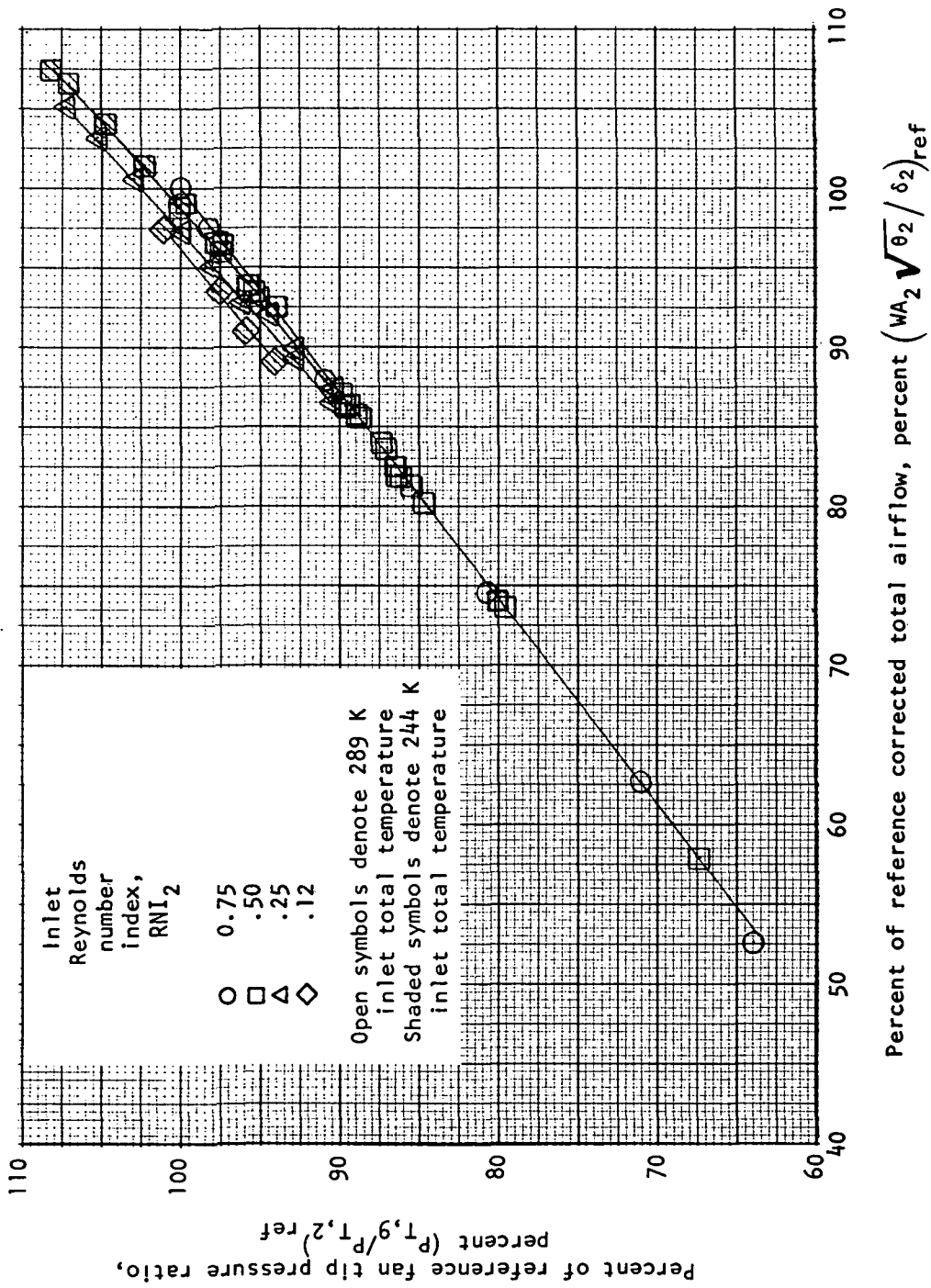
(c) Fan tip operating lines.

Figure 3. - Continued.
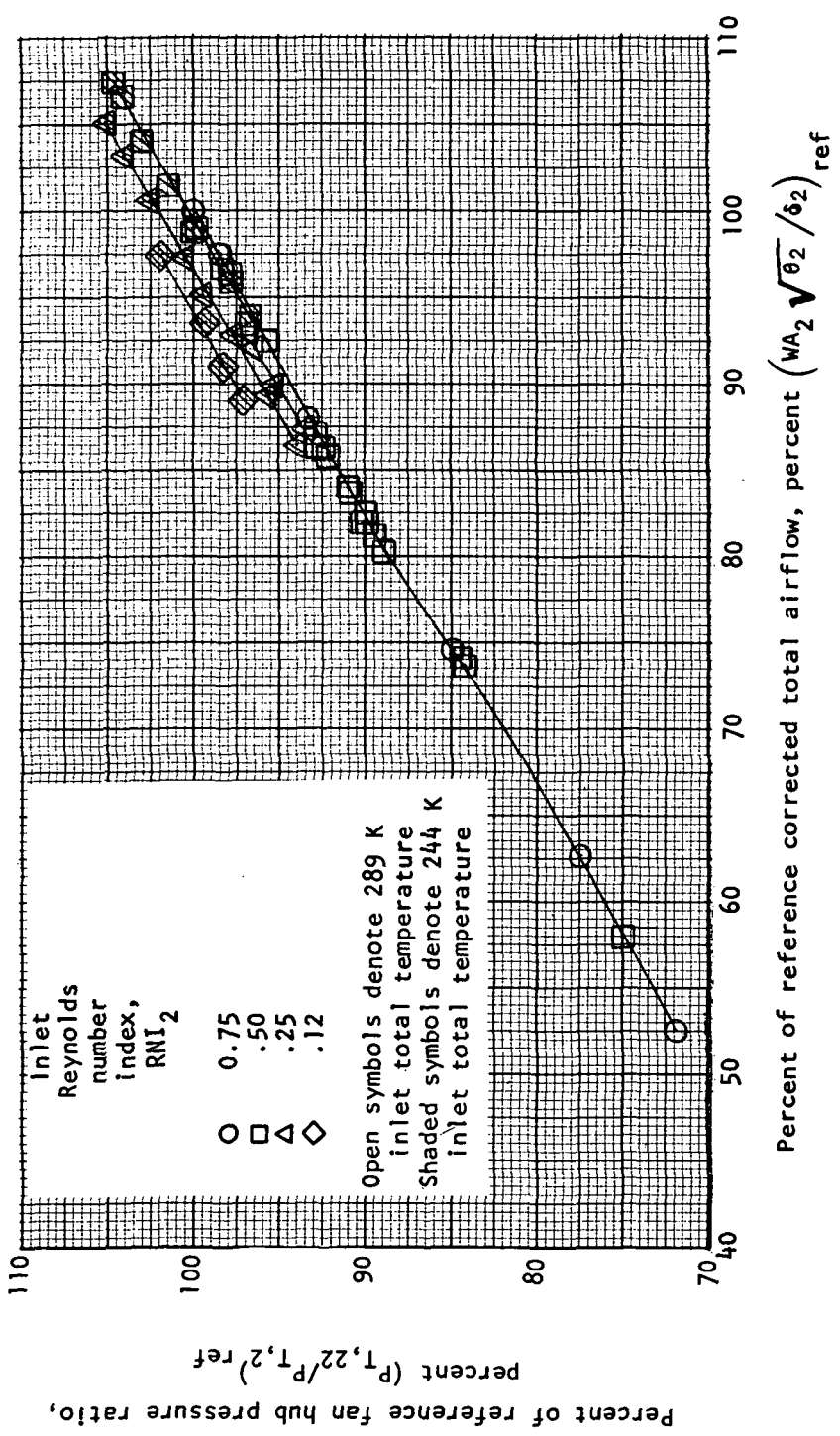
(d) Fan hub operating lines.

Figure 3. - Continued.

22

Percent of reference corrected fan speed, percent $\left(NF/\sqrt{\theta_2}\right)_{ref}$
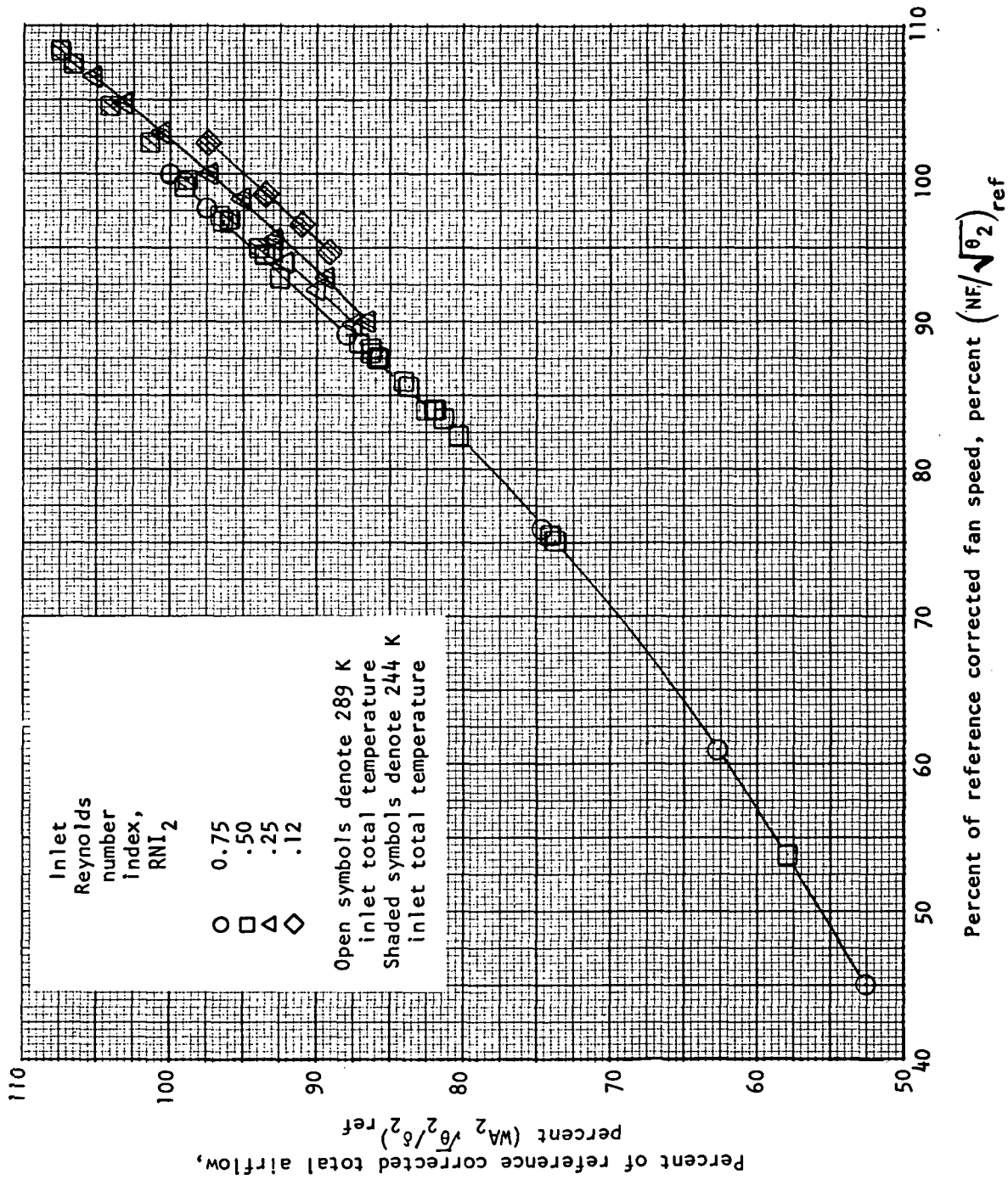
(e) Corrected total airflow plotted against corrected fan speed.

Figure 3. – Continued.

Percent of reference corrected total airflow, percent $\left(WA_2\sqrt{\theta_2}/\delta_2\right)_{ref}$

Inlet Reynolds number index, RNI_2

○ 0.75
□ .50
△ .25
◇ .12

Open symbols denote 289 K inlet total temperature
Shaded symbols denote 244 K inlet total temperature
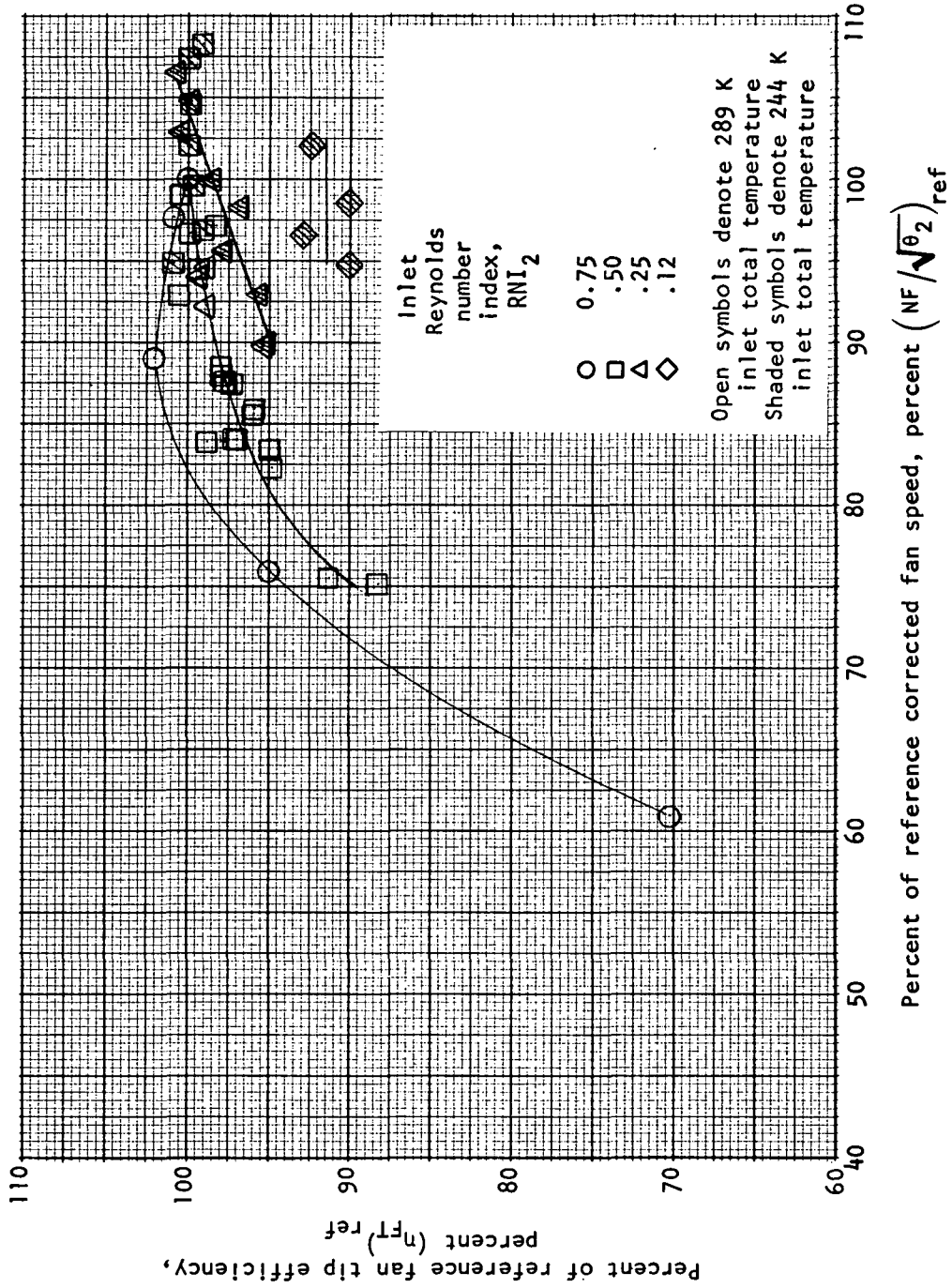
(f) Fan tip efficiency plotted against corrected fan speed.

Figure 3. - Continued.

24
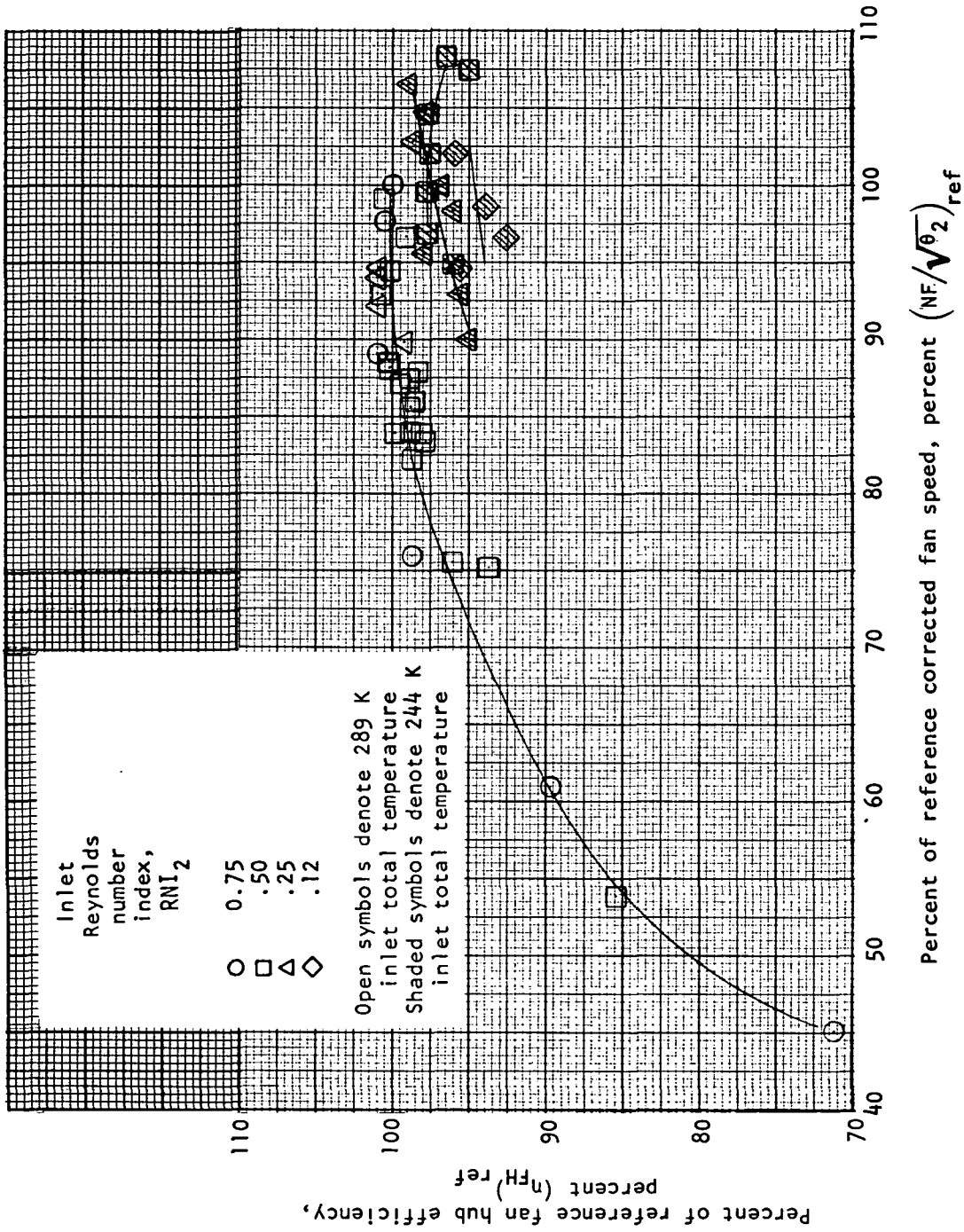
(g) Fan hub efficiency plotted against corrected fan speed.
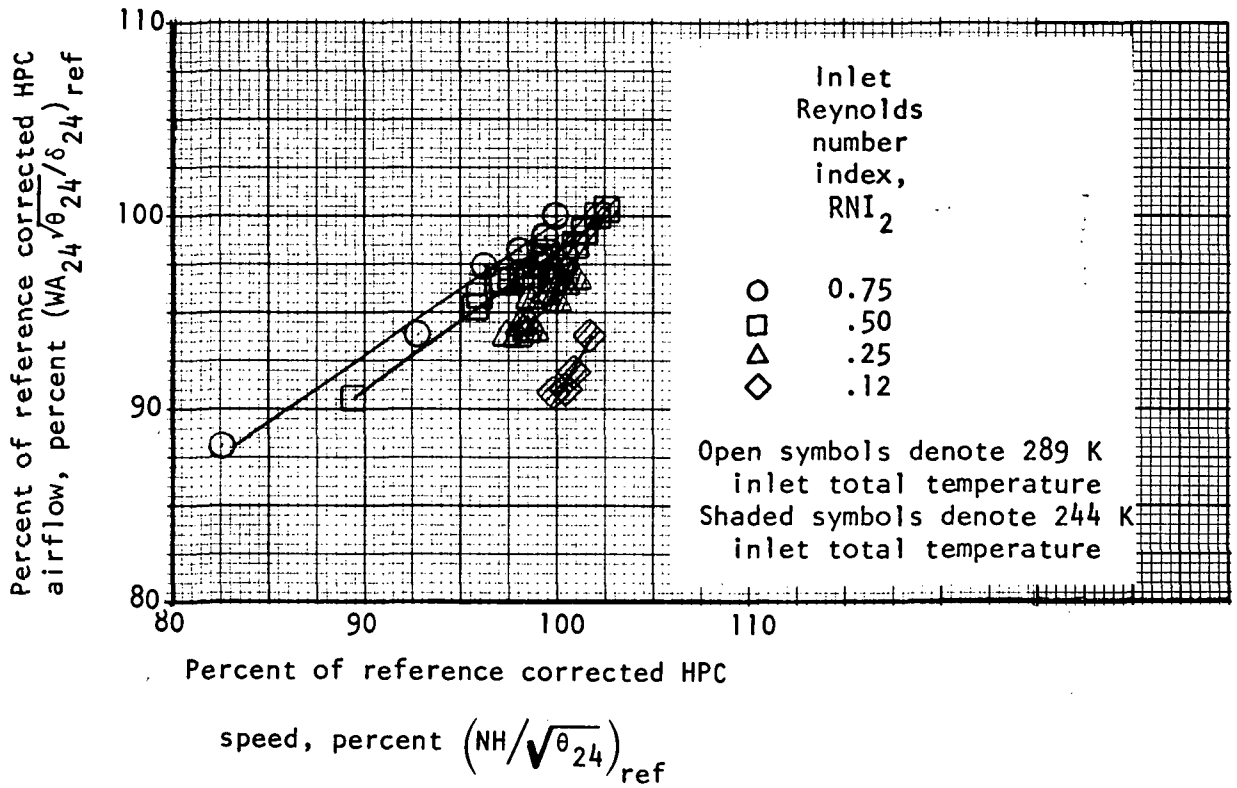
Figure 3. – Concluded.

25
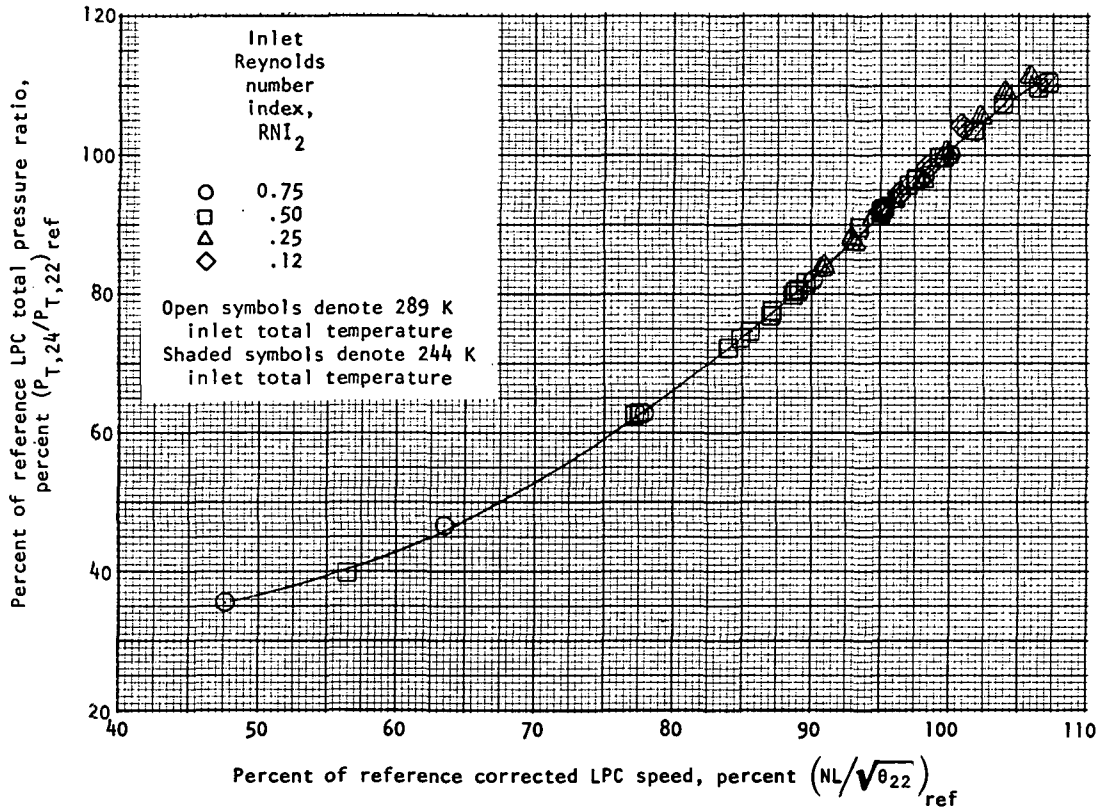
(a) LPC pressure ratio plotted against corrected LPC speed.

Figure 4.-Low pressure compressor (LPC) performance at simulated Mach number $M_0 = 0.8$.
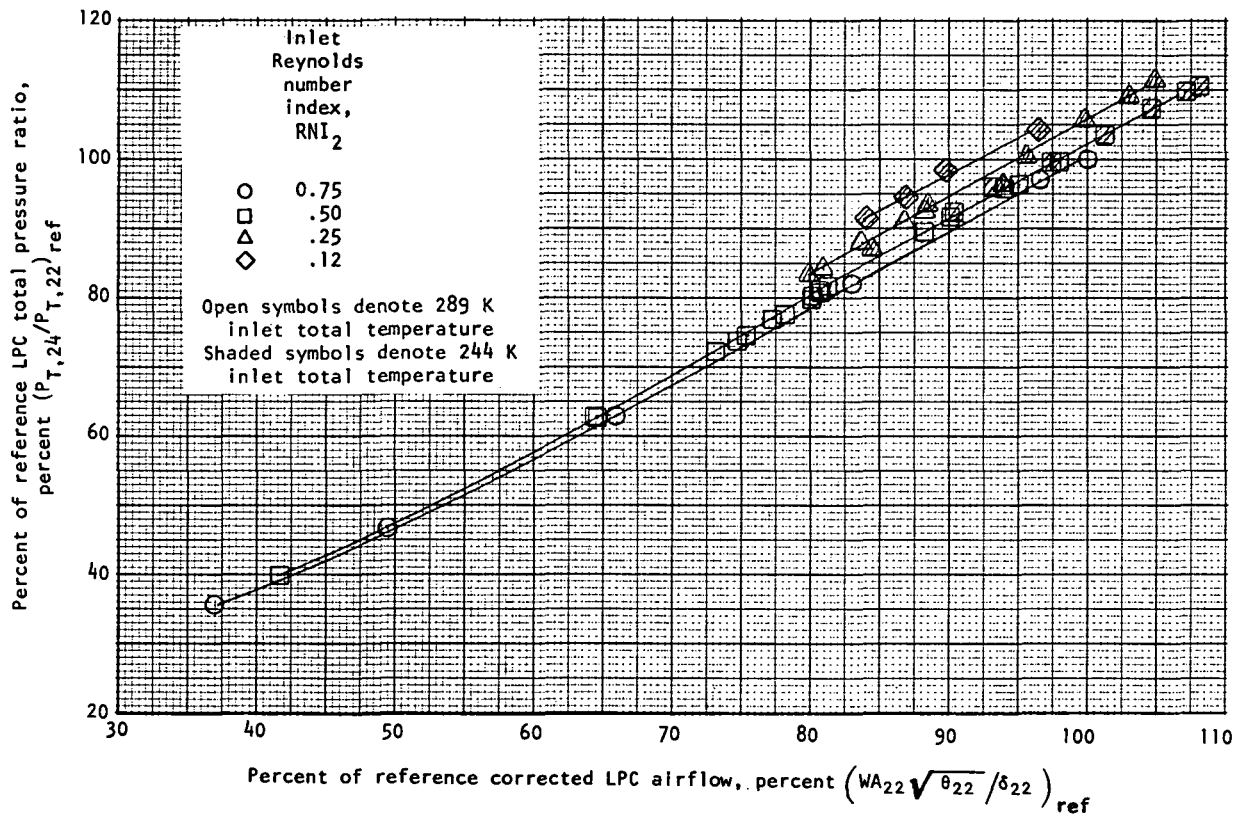
(b) Operating lines.

Figure 4. - Continued.
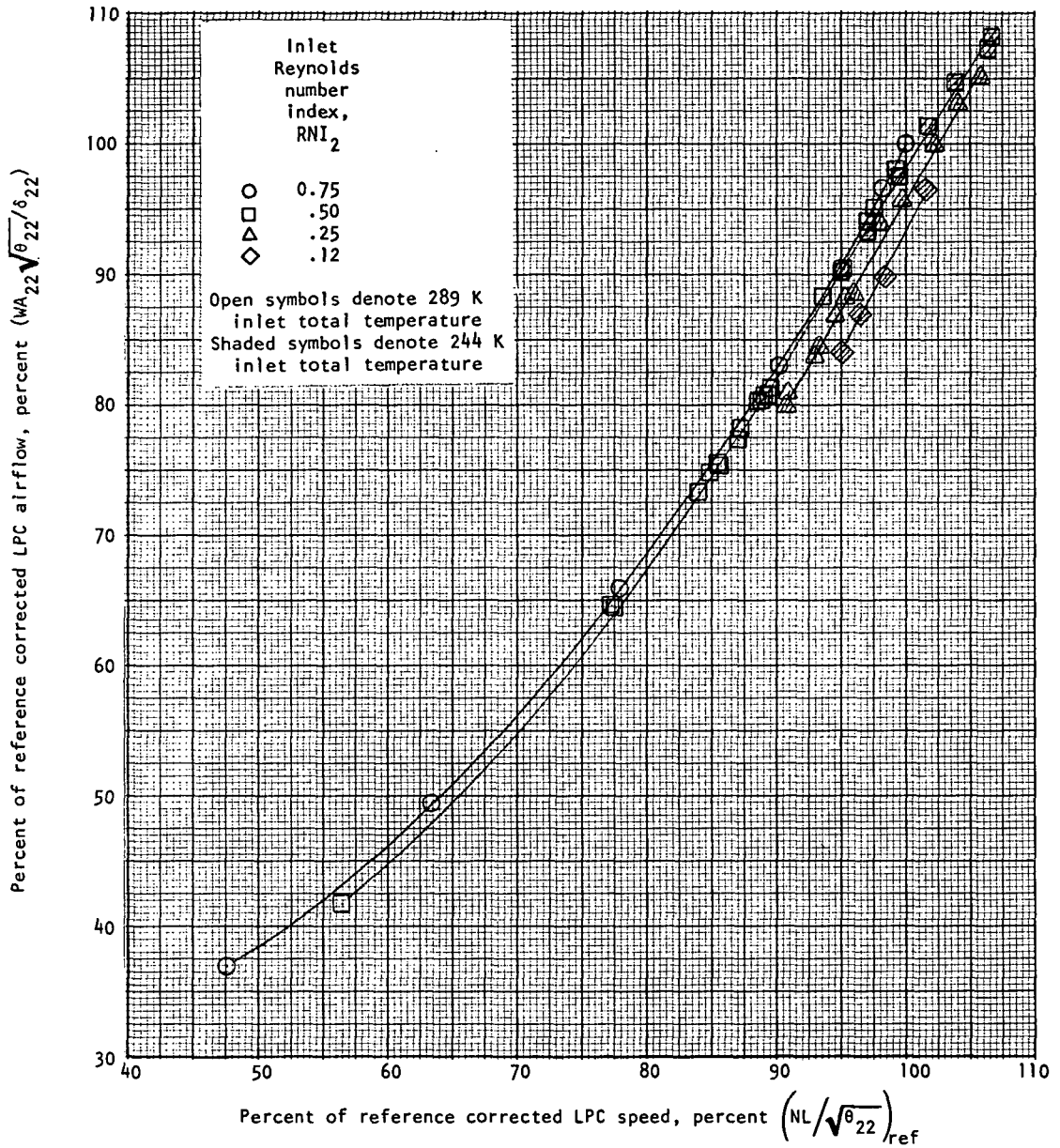
(c) Corrected airflow plotted against corrected LPC speed.
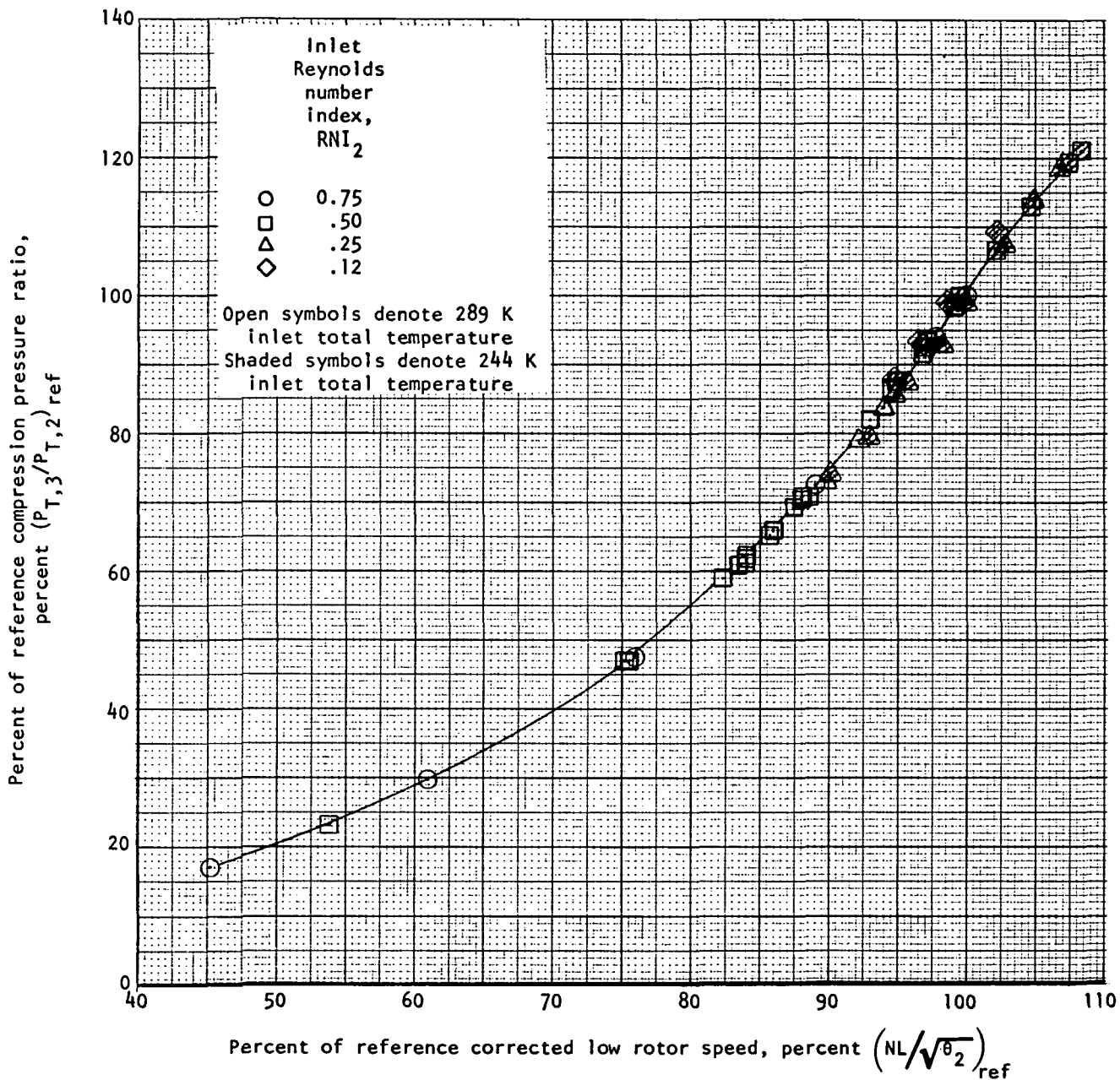
Figure 4. – Continued.

Inlet
Reynolds
number
index,
RNI_2

○   0.75
□   .50
△   .25
◇   .12

Open symbols denote 289 K
 inlet total temperature
Shaded symbols denote 244 K
 inlet total temperature
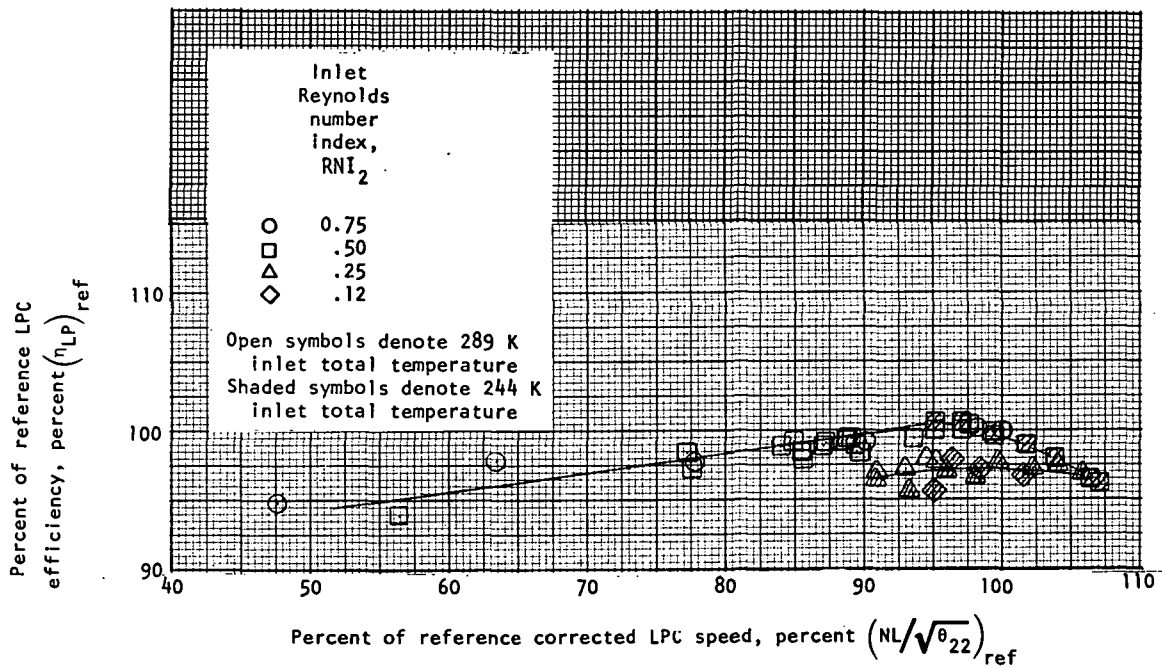
(d) LPC efficiency plotted against corrected LPC speed.

Figure 4. - Concluded.
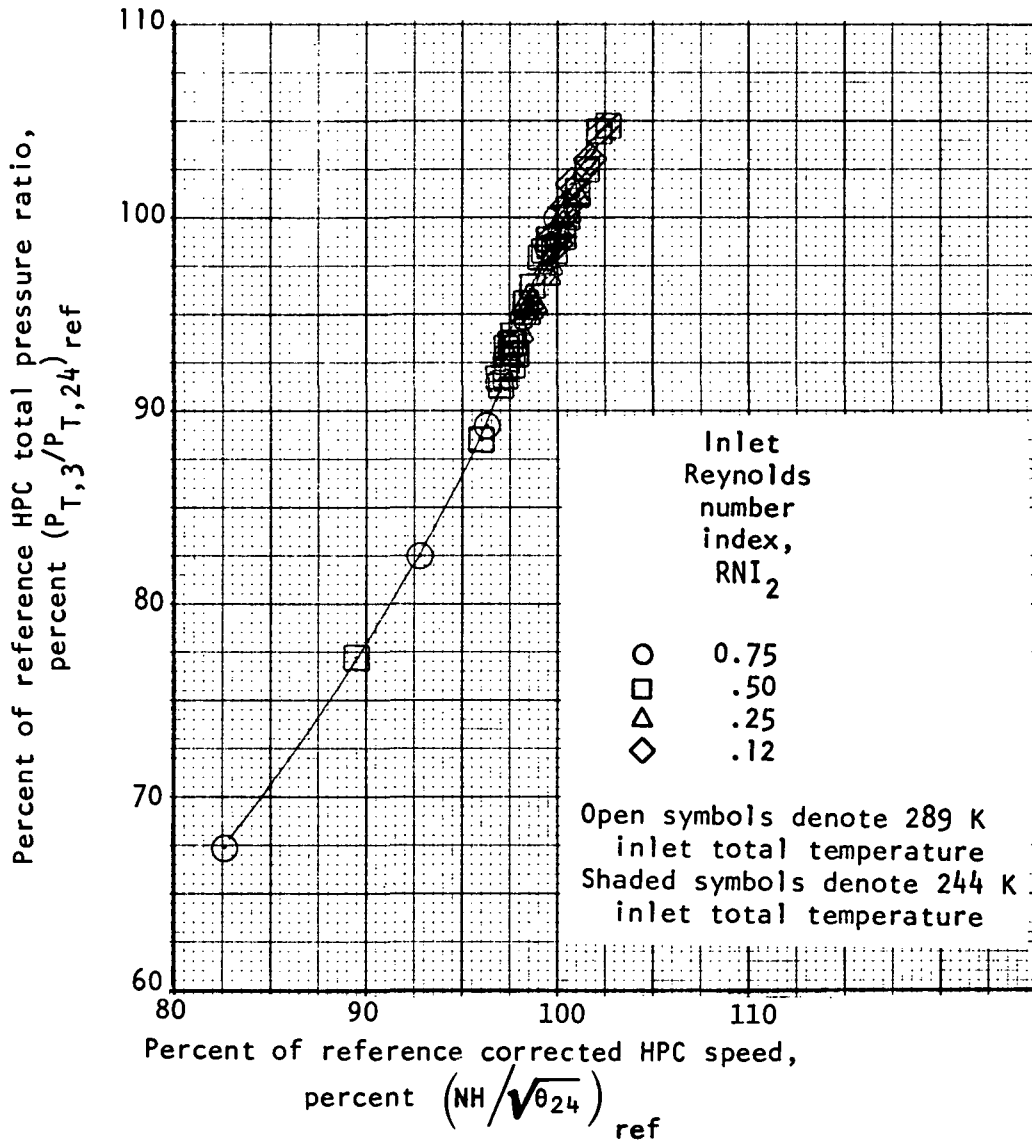
(a) HPC pressure ratio plotted against corrected HPC speed.

Figure 5. - High pressure compressor performance at simulated Mach number $M_0 = 0.8$.

Percent of reference HPC total pressure ratio, percent $\left(P_{T,3}/P_{T,24}\right)_{ref}$

Percent of reference corrected HPC airflow, percent $\left(WA_{24}\sqrt{.\theta_{24}}/\delta_{24}\right)_{ref}$

Inlet
Reynolds
number
index,
RNI_2

○	0.75
□	.50
△	.25
◇	.12

Open symbols denote 289 K
inlet total temperature
Shaded symbols denote 244 K
inlet total temperature
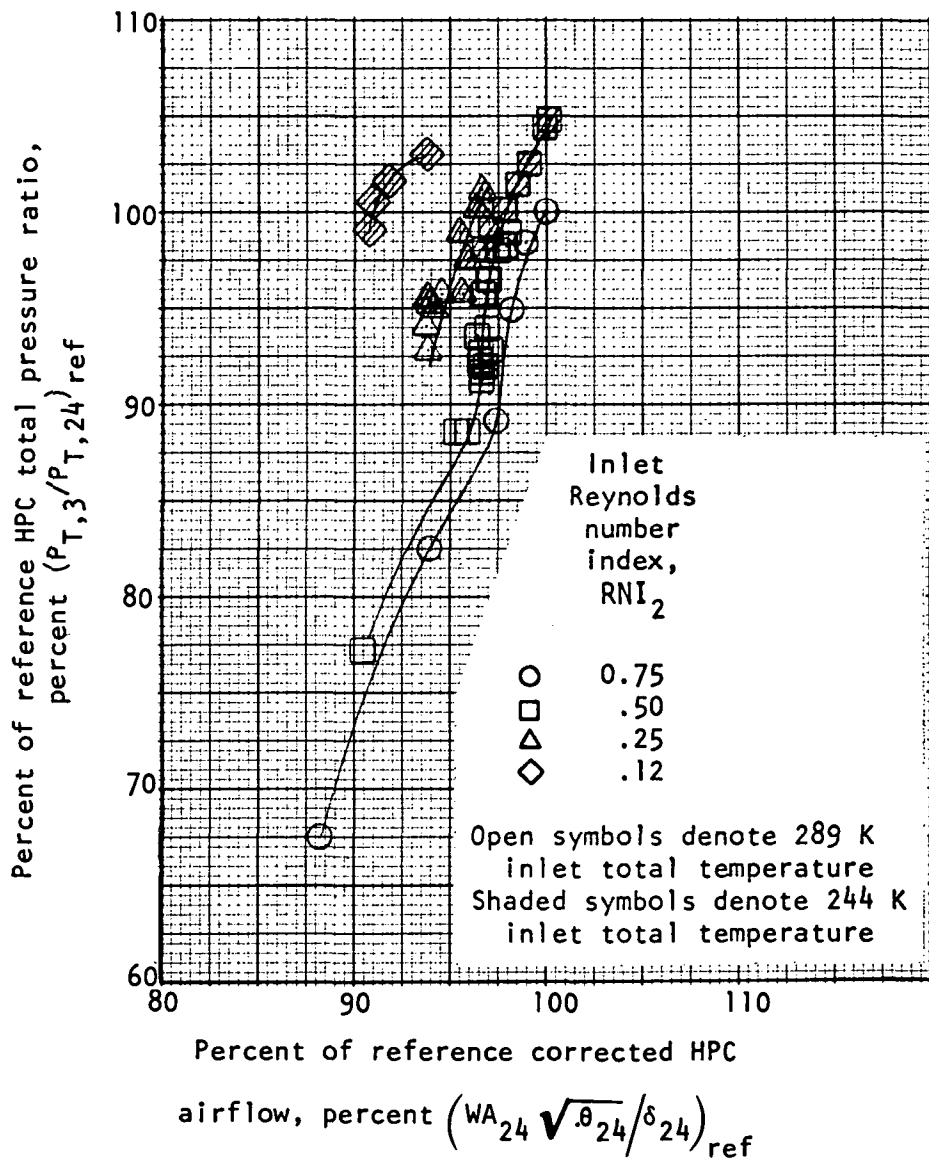
(b) Operating line

Figure 5. - Continued.

(c) Corrected airflow plotted against corrected HPC speed.

Figure 5. - Continued.
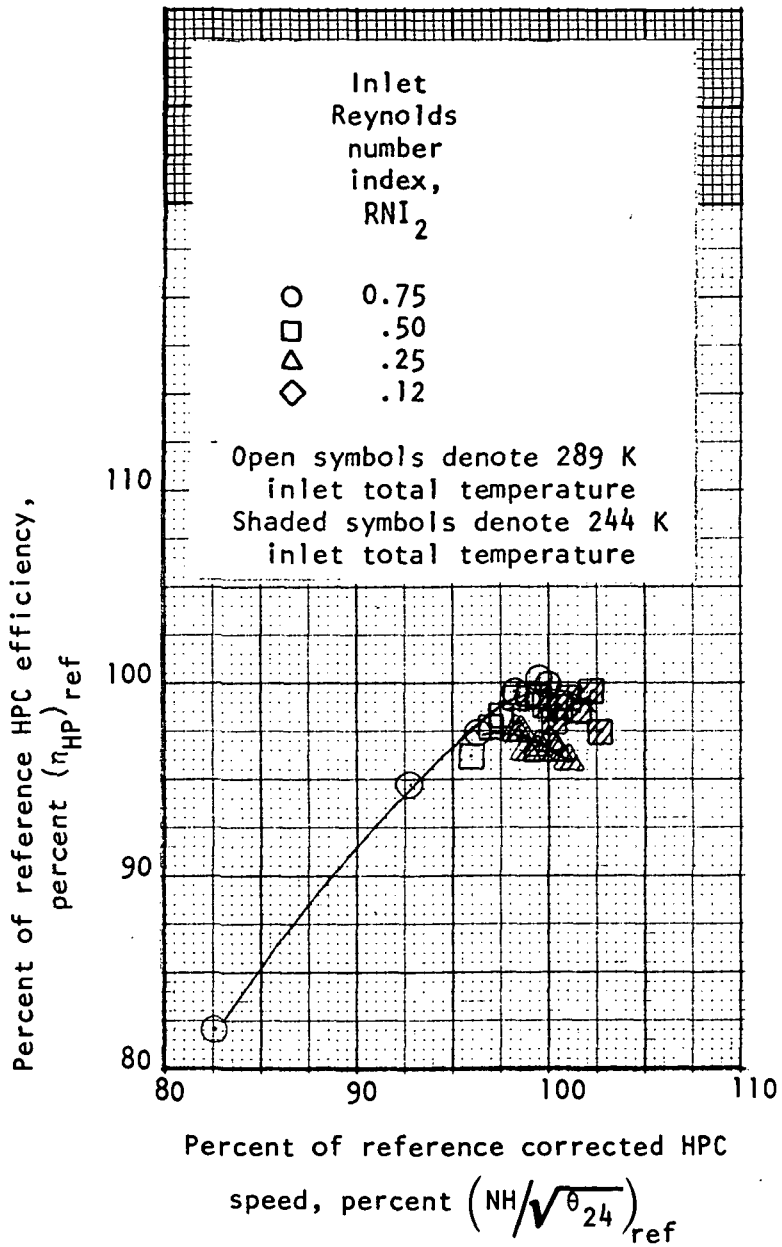
(d) HPC efficiency plotted against corrected HPC speed.

Figure 5. - Concluded.

Percent of reference corrected low rotor speed, percent $\left(NL/\sqrt{\theta_2}\right)_{ref}$
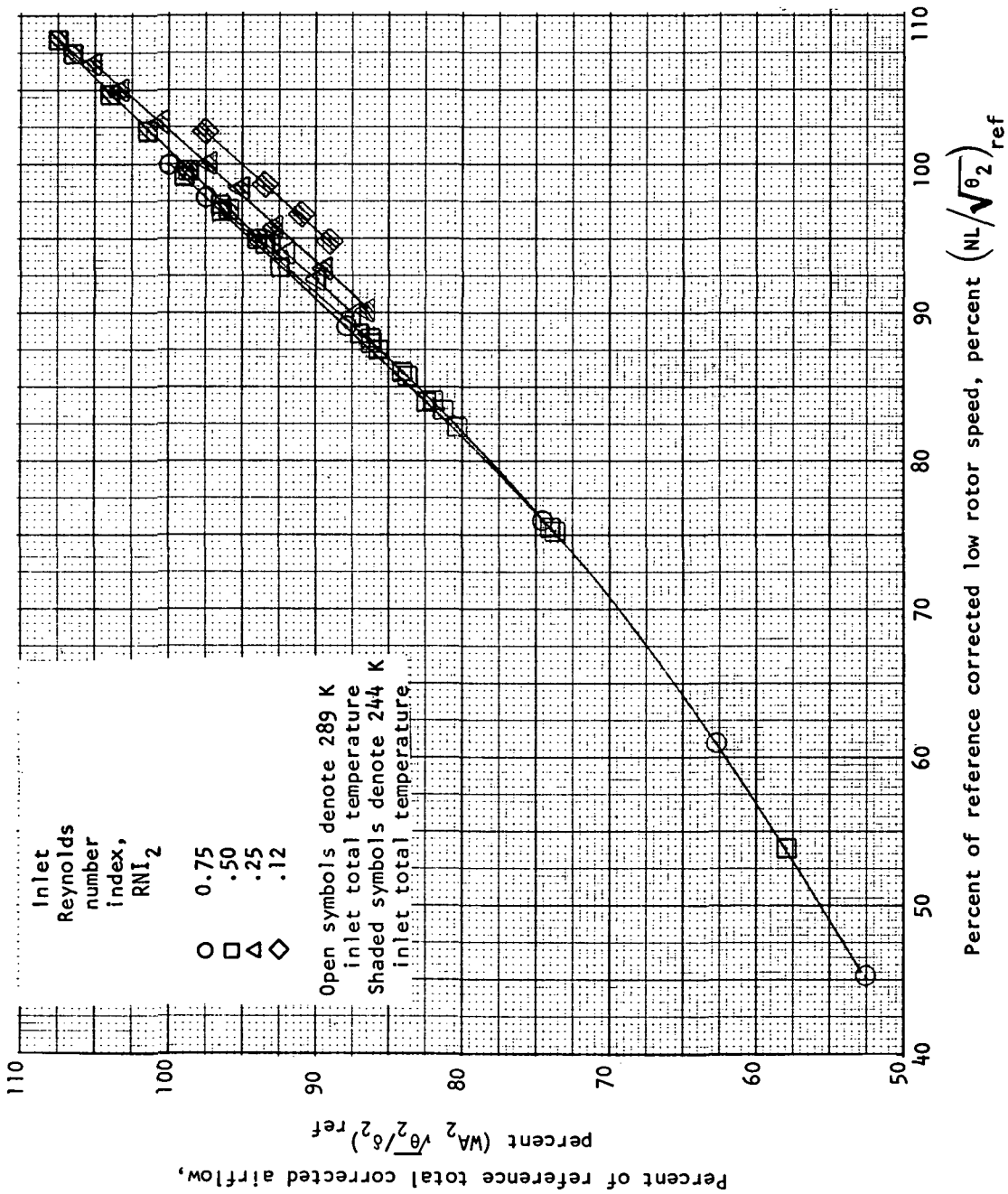
(a) Corrected airflow plotted against corrected low rotor speed.

Figure 6. – Compression system overall performance at simulated Mach number $M_0 = 0.8$.
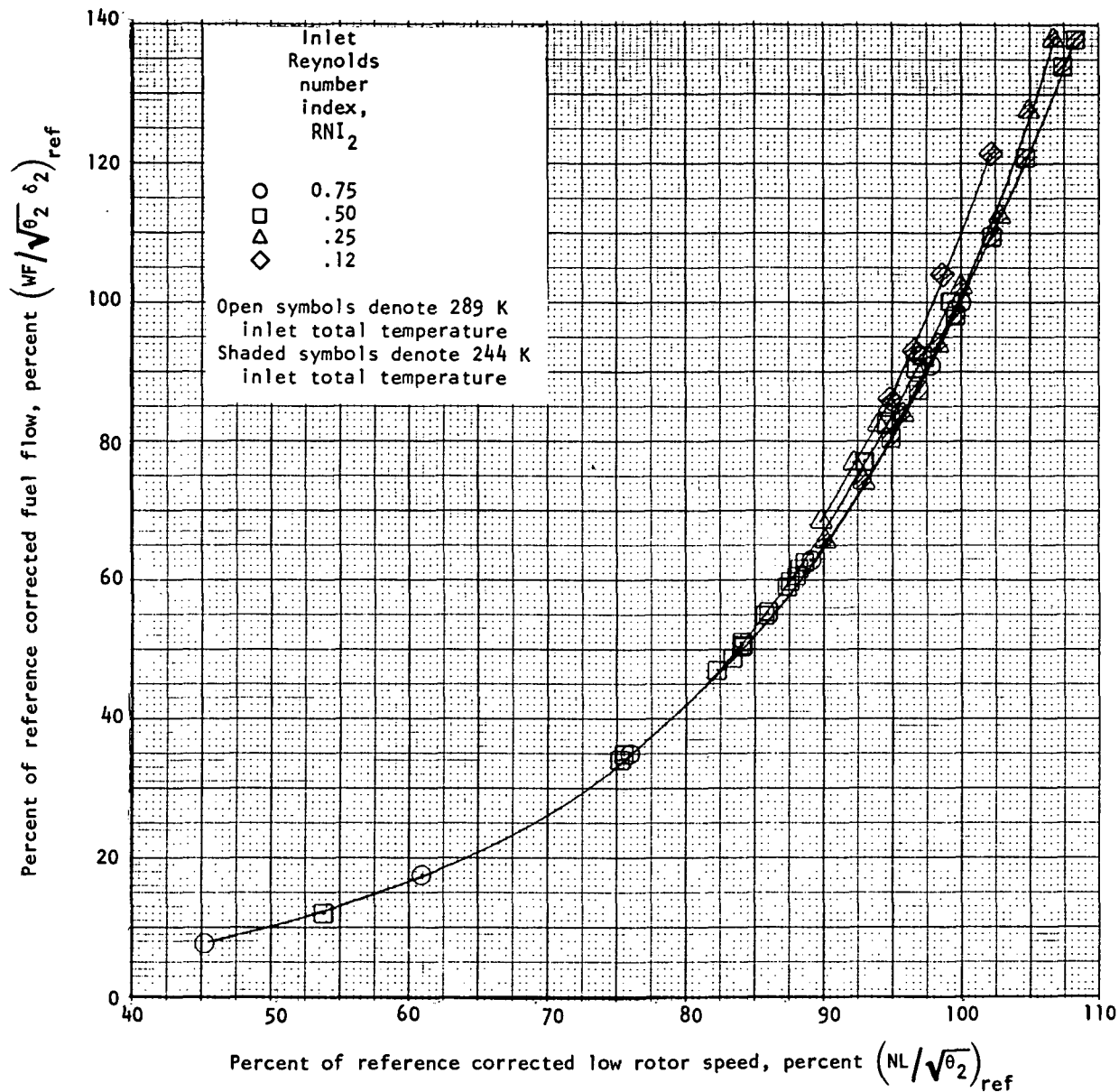
(b) Overall pressure ratio plotted against corrected low rotor speed.

Figure 6. - Continued.

Inlet
Reynolds
number
index,
RNI_2

○   0.75
□   .50
△   .25
◇   .12

Open symbols denote 289 K
inlet total temperature
Shaded symbols denote 244 K
inlet total temperature

Percent of reference compression temperature ratio, percent $\left(T_{T,3}/T_{T,2}\right)_{ref}$

Percent of reference corrected low rotor speed, percent $\left(NL\Big/\sqrt{\theta_2}\right)_{ref}$
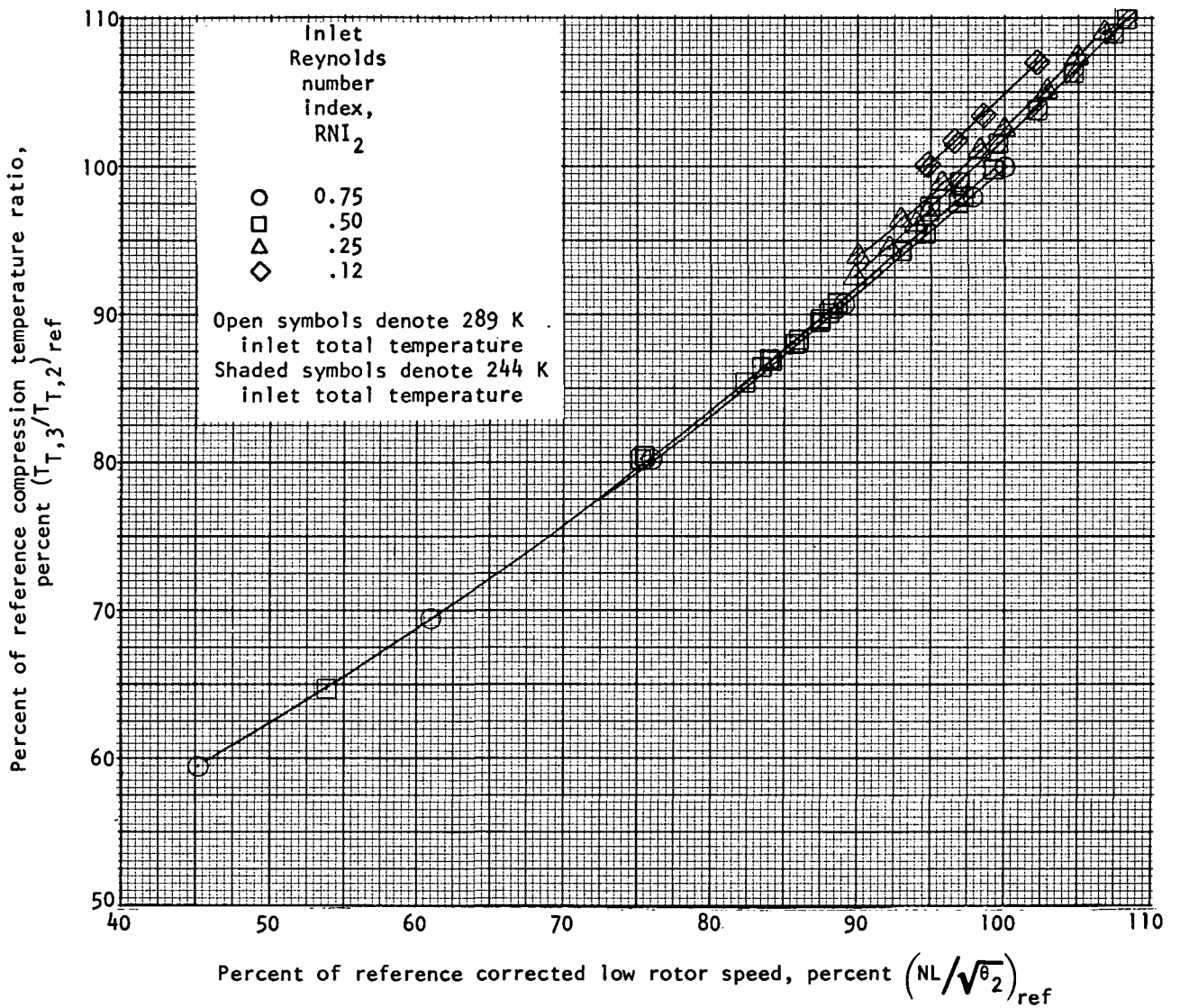
(c) Overall temperature ratio plotted against corrected low rotor speed.

Figure 6. - Concluded.

(a) Corrected fuel flow plotted against corrected low rotor speed.

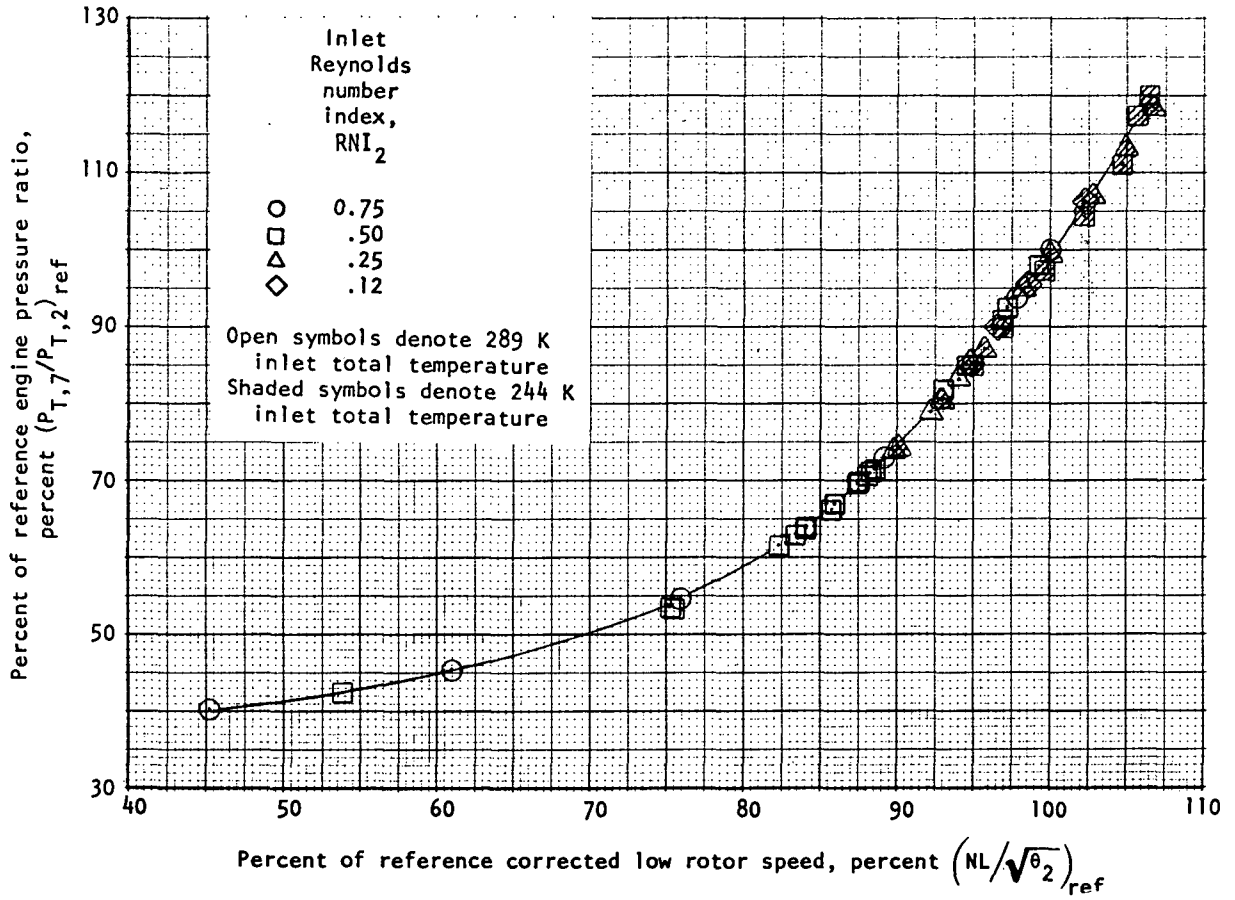Figure 7. - Energy requirements at simulated Mach number $M_0 = 0.8$.
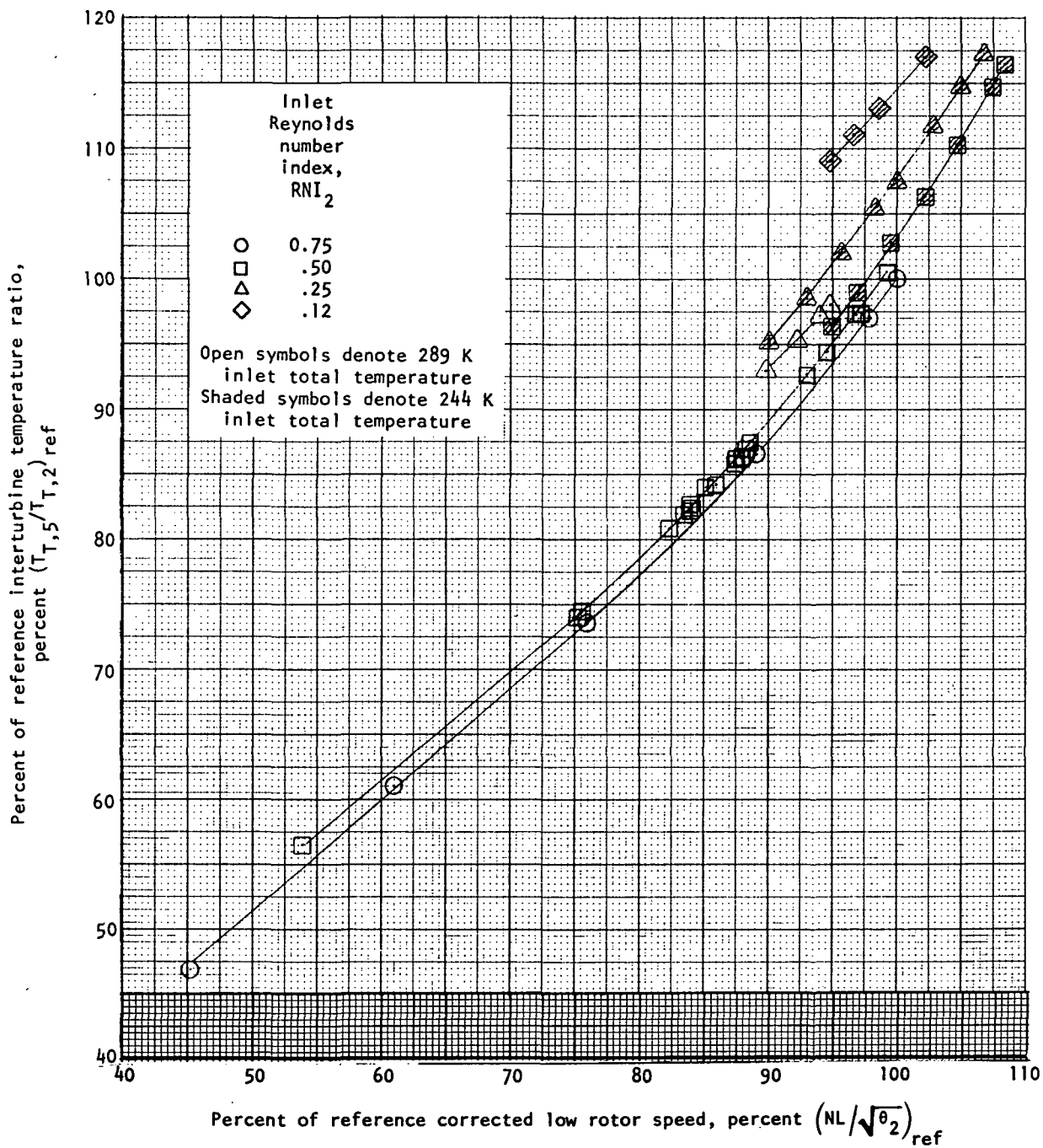
(b) Inter-turbine temperature ratio plotted against corrected low rotor speed.
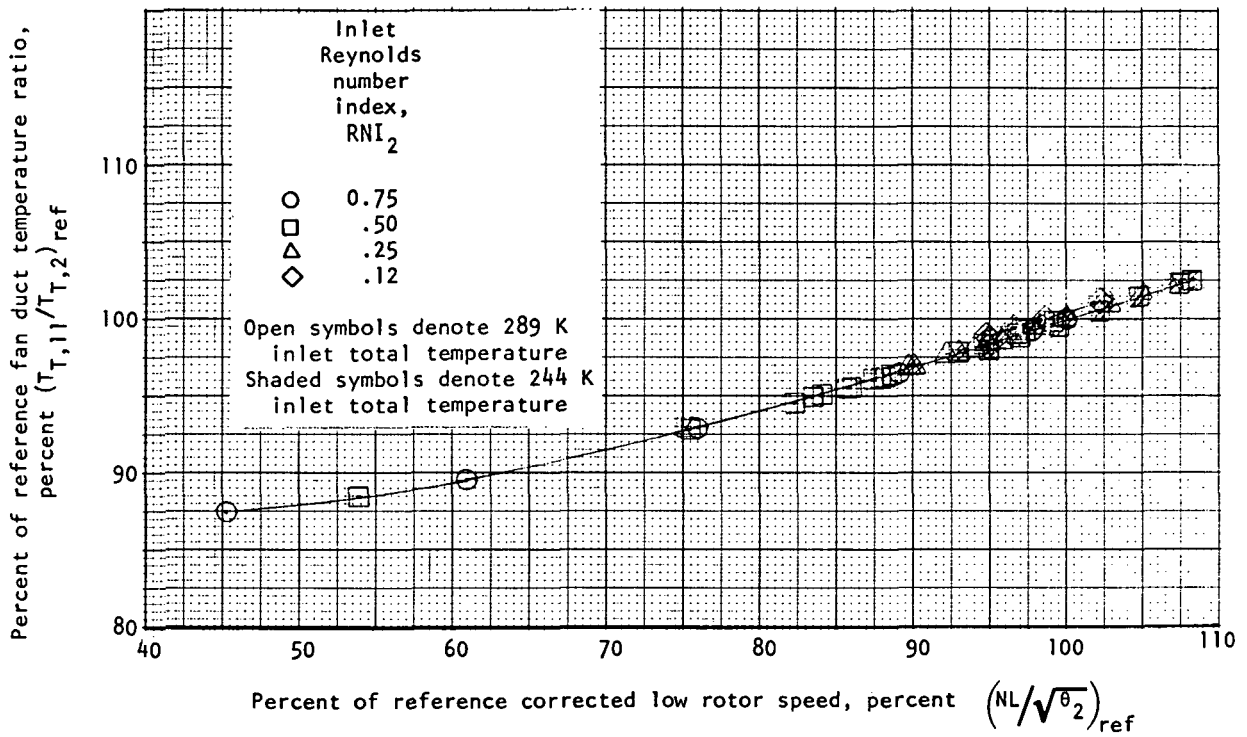
Figure 7. - Concluded.
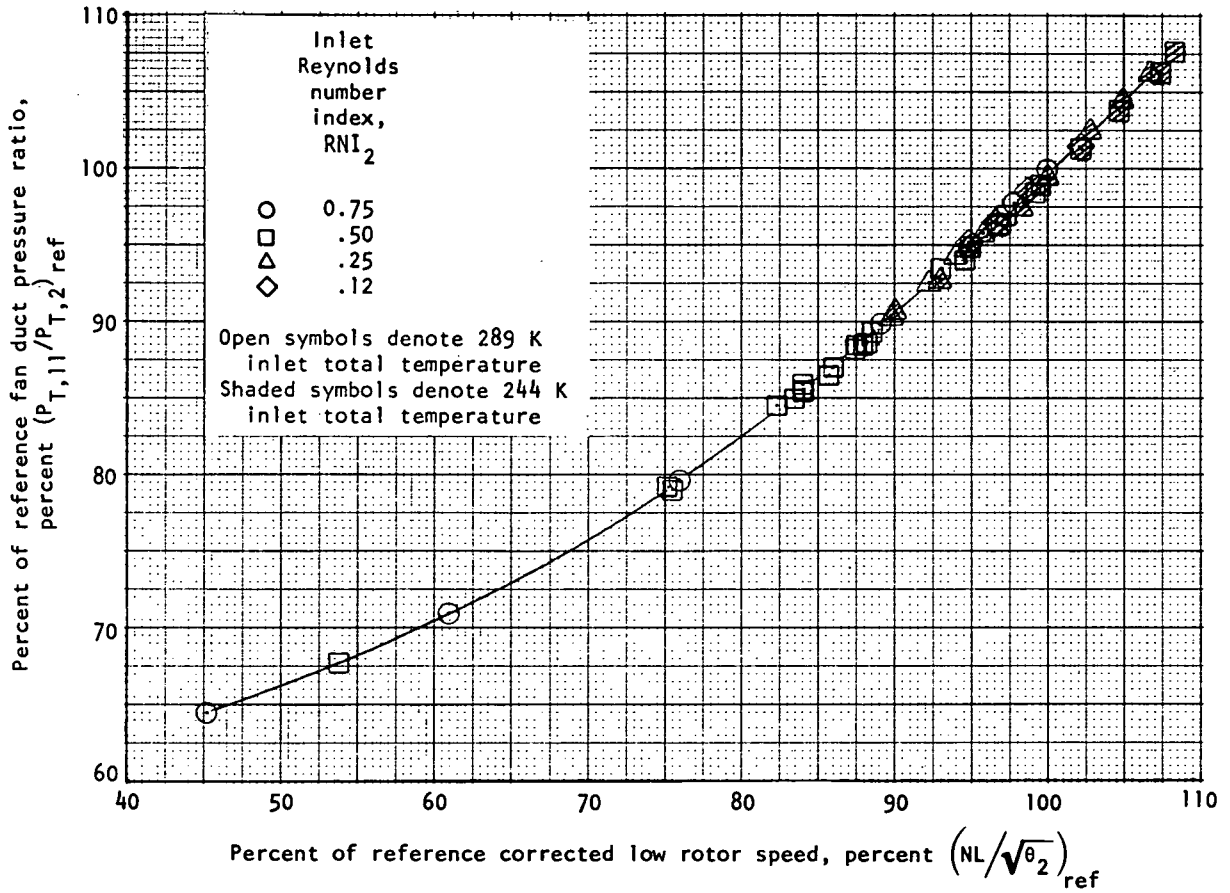
(a) Fan Duct pressure ratio plotted against corrected low rotor speed.

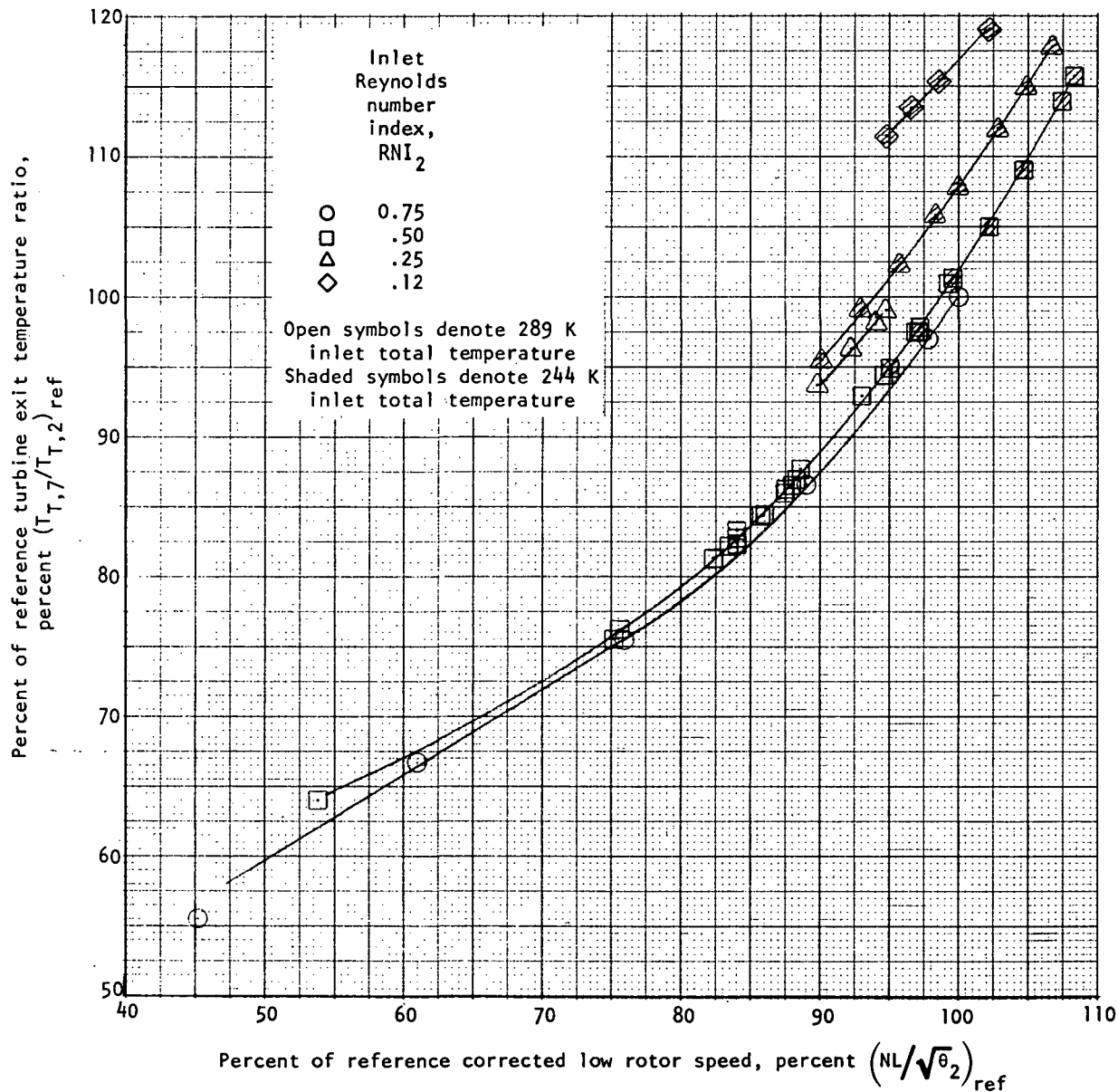Figure 8. - Overall cycle performance at simulated Mach number M_0 = 0.8.

(b) Engine pressure ratio plotted against corrected low rotor speed.
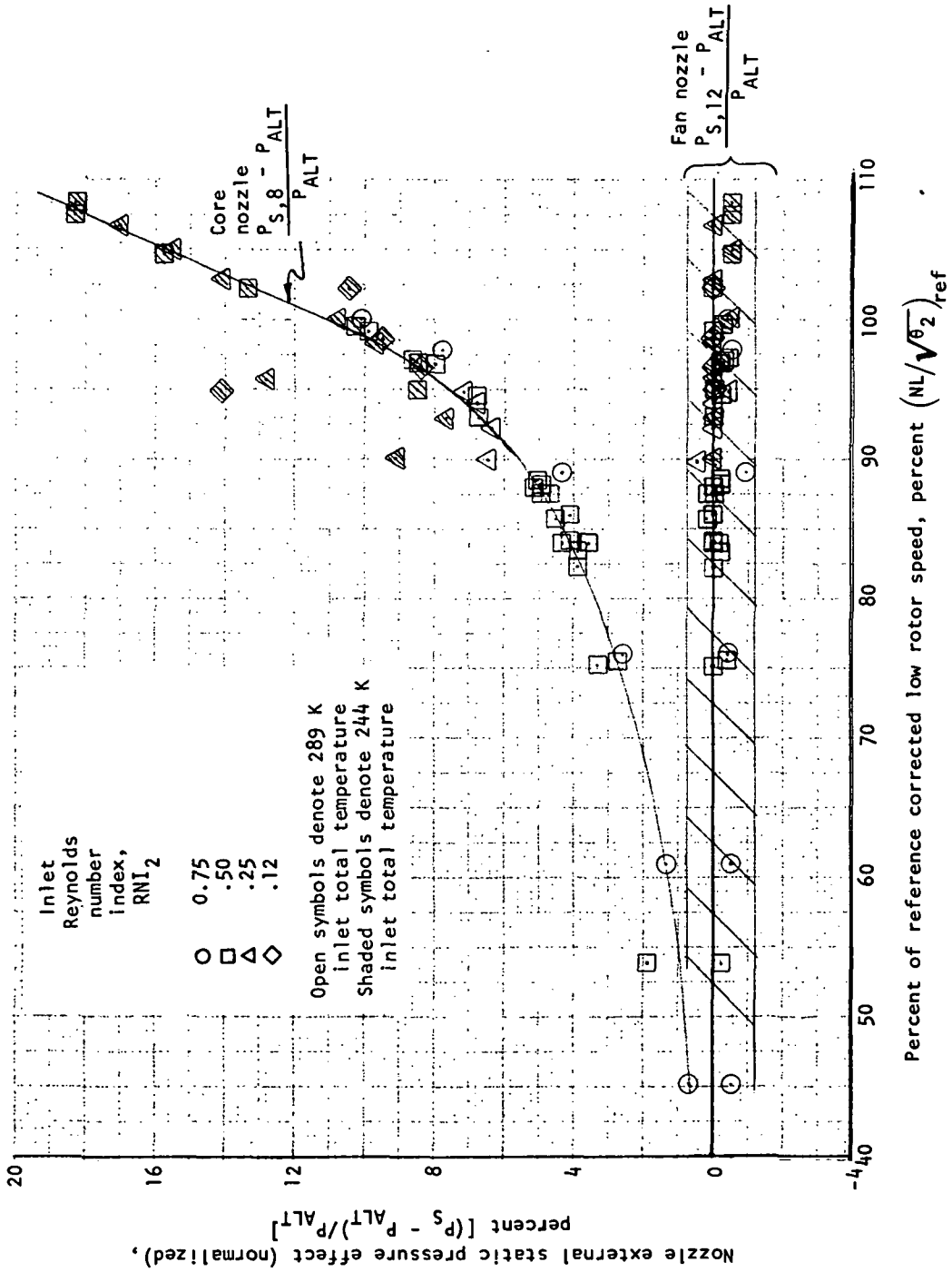
Figure 8. - Continued.

Percent of reference fan duct temperature ratio, percent $(T_{T,11}/T_{T,2})_{ref}$

Percent of reference corrected low rotor speed, percent $\left(N_L/\sqrt{\theta_2}\right)_{ref}$

Inlet
Reynolds
number
index,
RNI_2

○　0.75
□　.50
△　.25
◇　.12

Open symbols denote 289 K
inlet total temperature
Shaded symbols denote 244 K
inlet total temperature

110

100

90

80

40　50　60　70　80　90　100　110

(c) Fan duct temperature ratio plotted against corrected low rotor speed.

Figure 8. - Continued.

(d) Turbine exit temperature ratio plotted against corrected low rotor speed.

Figure 8. - Concluded.
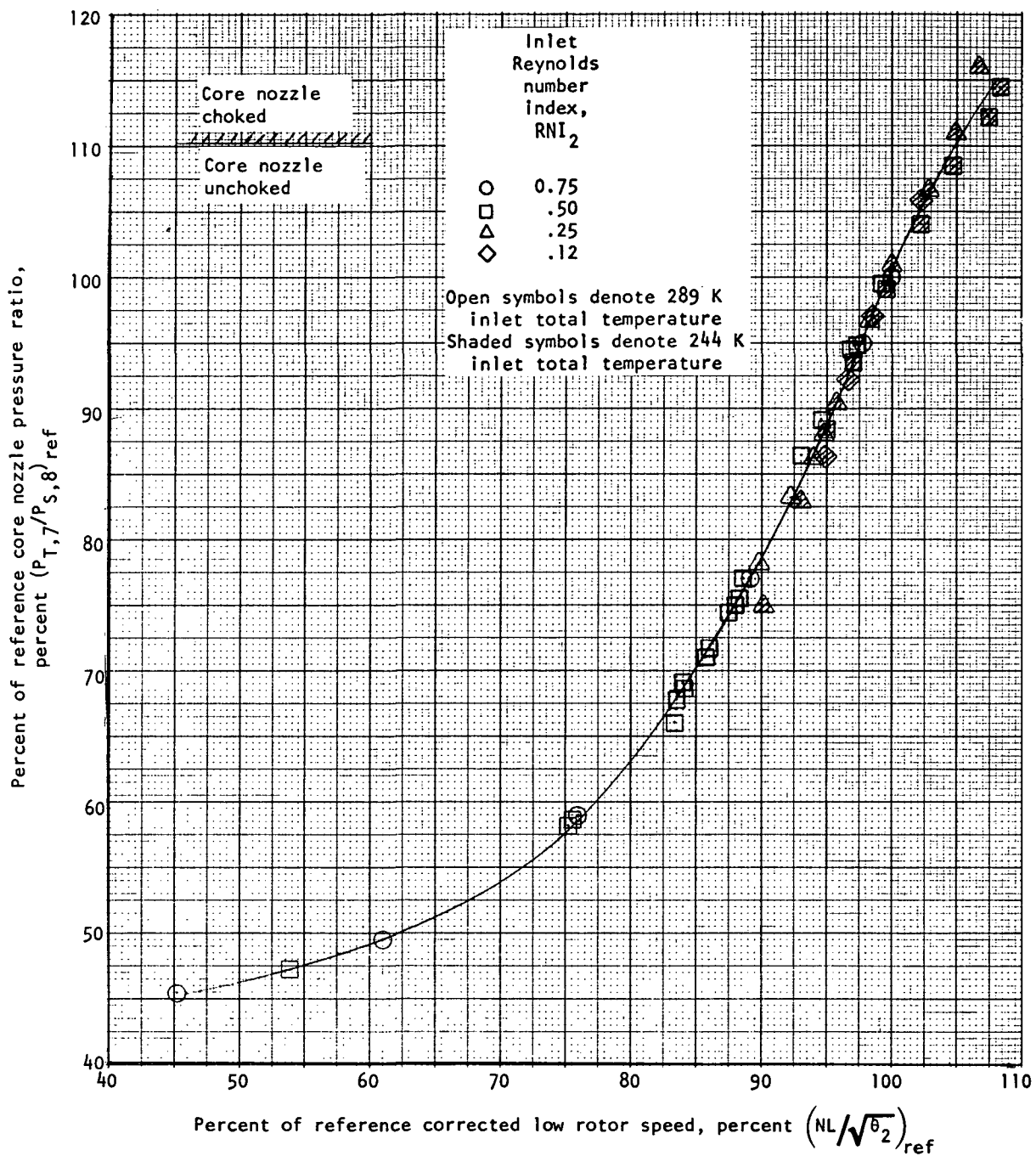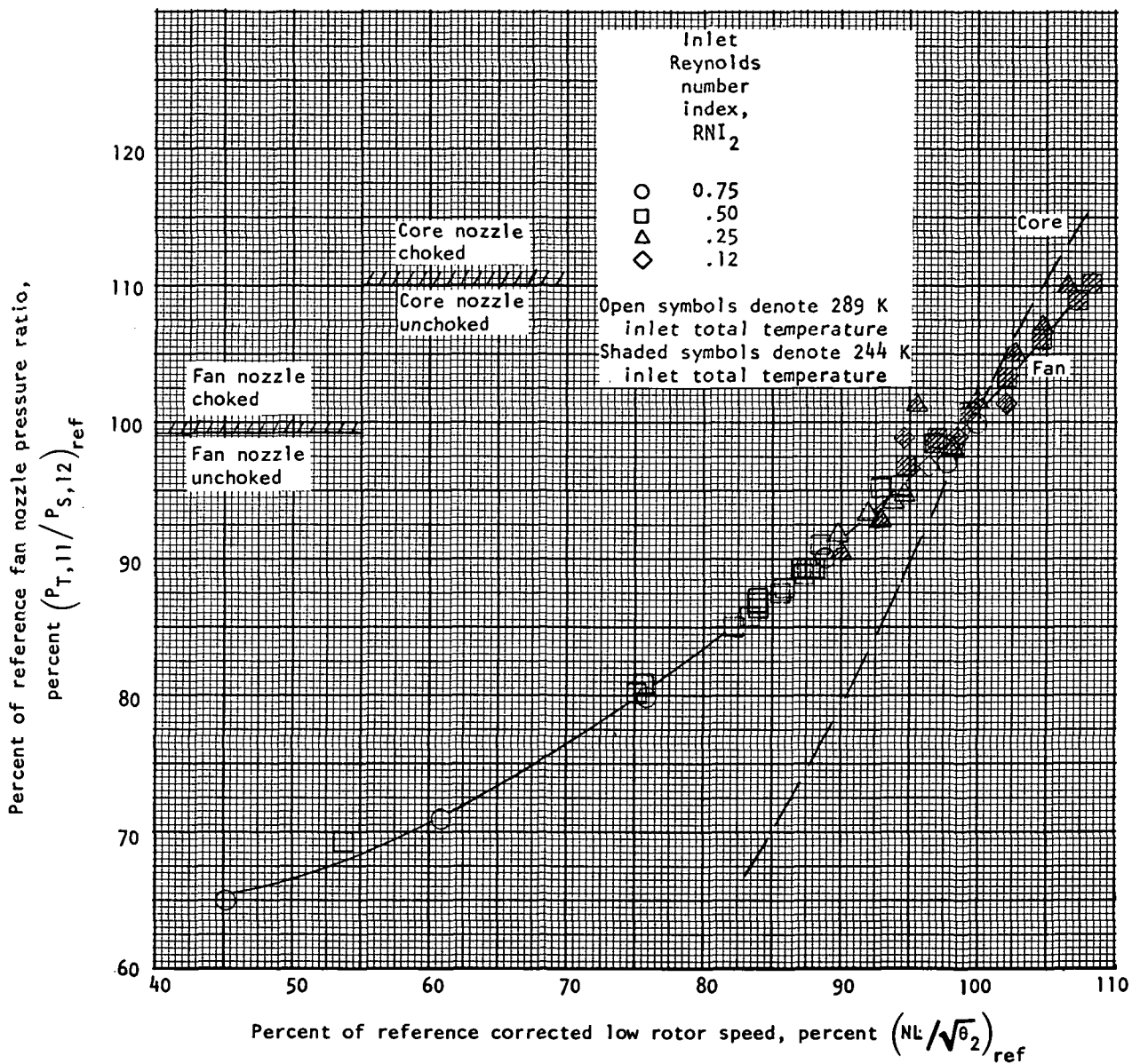
Core nozzle $\dfrac{P_{S,8} - P_{ALT}}{P_{ALT}}$

Fan nozzle $\dfrac{P_{S,12} - P_{ALT}}{P_{ALT}}$

Percent of reference corrected low rotor speed, percent $\left(NL/\sqrt{\theta_2}\right)_{ref}$

(a) Effect of flow field on nozzle static pressure.

Figure 9. – Core and fan nozzle performance at simulated Mach number $M_0 = 0.8$.

Inlet
Reynolds
number
index,
RNI_2

○ 0.75
□ .50
△ .25
◇ .12

Open symbols denote 289 K
inlet total temperature
Shaded symbols denote 244 K
inlet total temperature

Nozzle external static pressure effect (normalized),
percent $[(P_S - P_{ALT})/P_{ALT}]$

20

16

12

8

4

0

-4

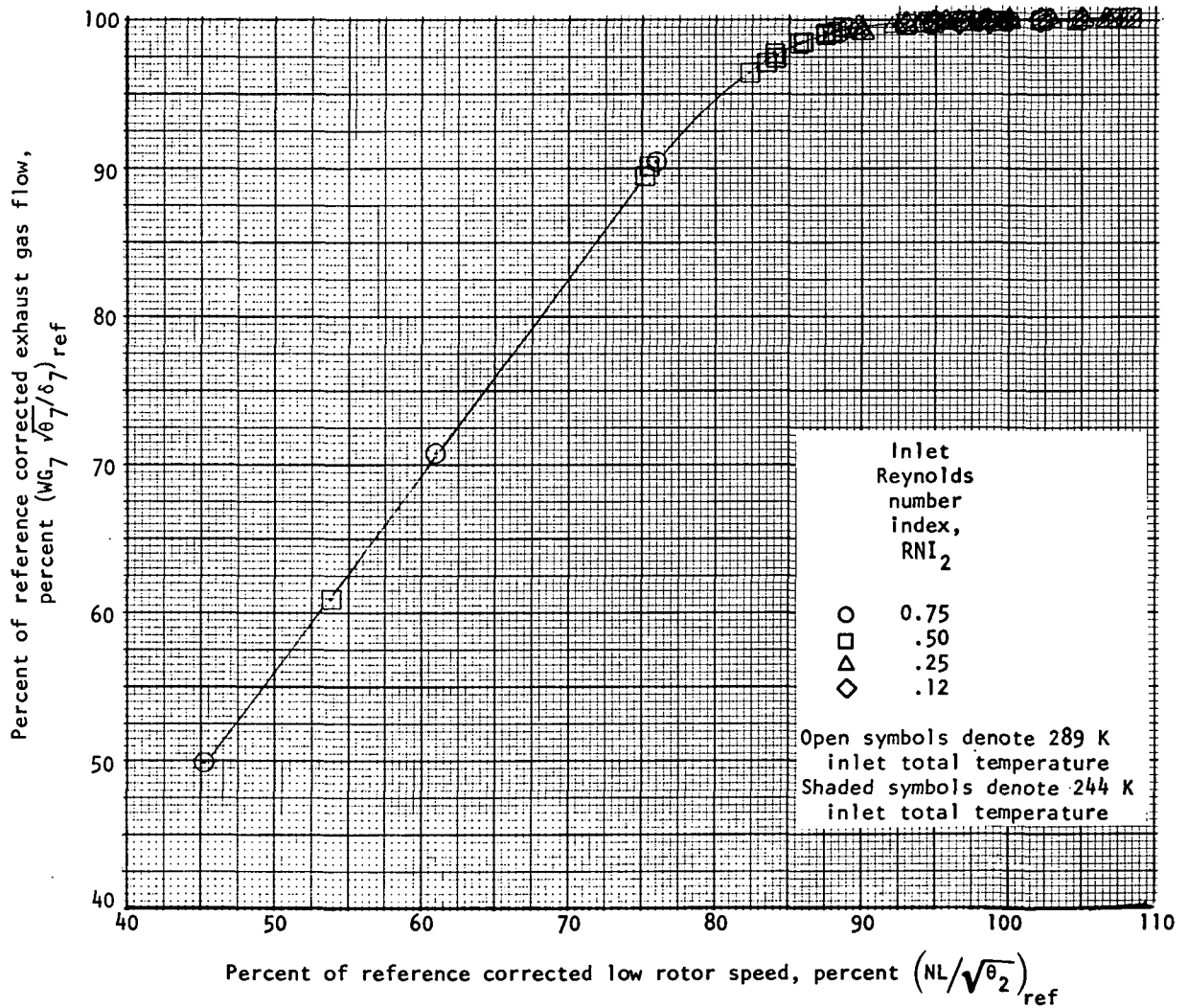40   50   60   70   80   90   100   110

(b) Core nozzle pressure ratio plotted against corrected low rotor speed.
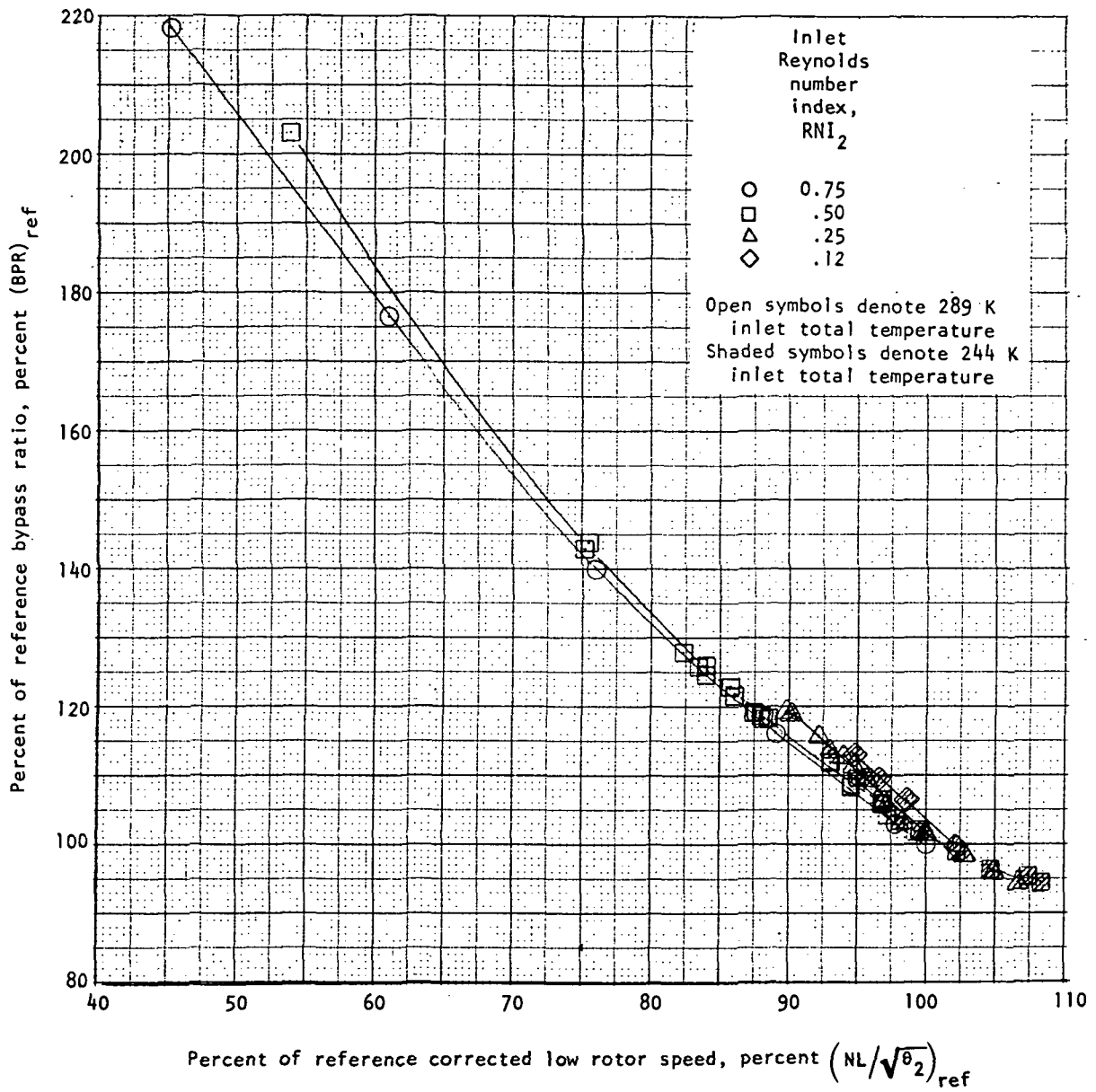
Figure 9. - Continued.

(c) Fan nozzle pressure ratio plotted against corrected low rotor speed.
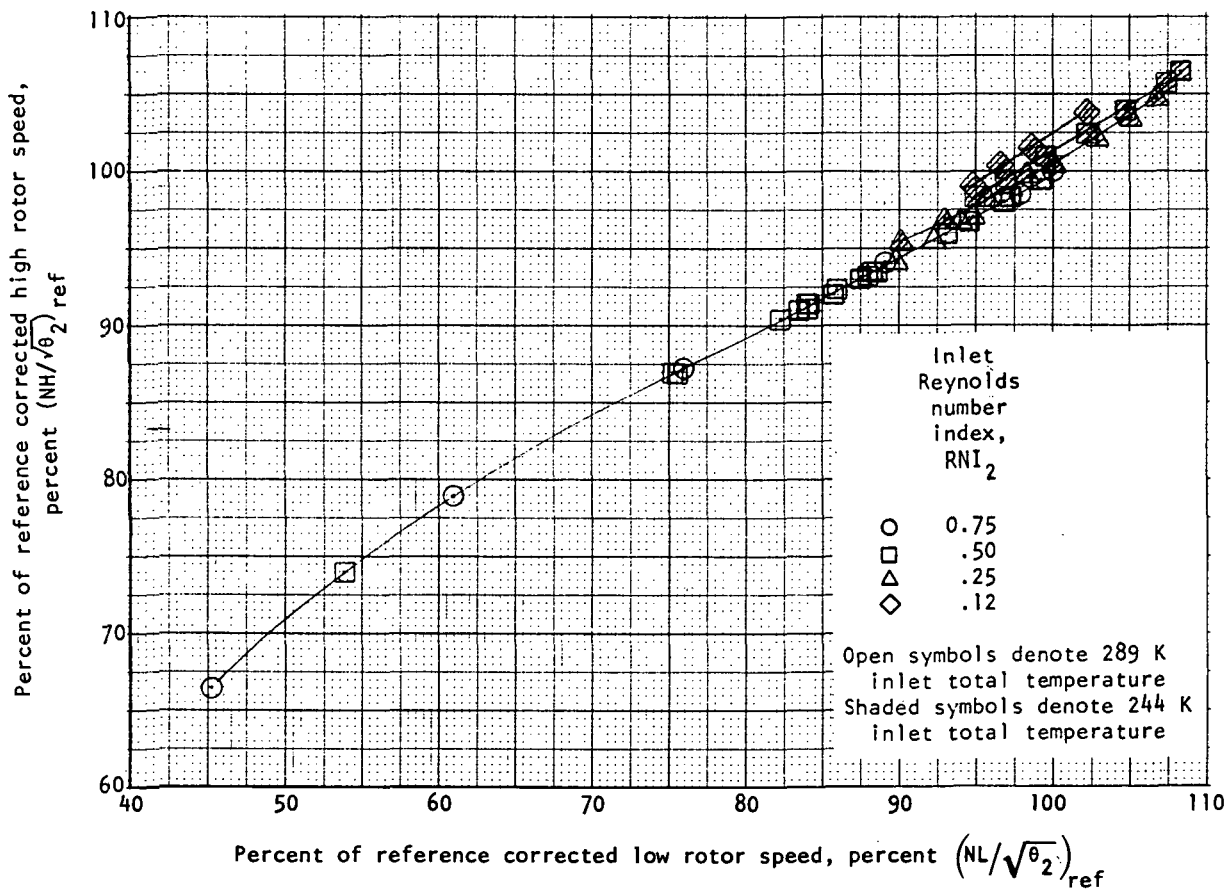
Figure 9. - Continued.

(d) Core nozzle corrected gas flow plotted against corrected low rotor speed.

Figure 9. - Concluded.

46

(a) Bypass ratio plotted against corrected low rotor speed.

Figure 10. - Flow split at simulated Mach number $M_0 = 0.8$.

(b) Speed match; corrected high rotor speed plotted against corrected low rotor speed.

Figure 10. – Concluded.

"The aeronautical and space activities of the United States shall be conducted so as to contribute . . . to the expansion of human knowledge of phenomena in the atmosphere and space. The Administration shall provide for the widest practicable and appropriate dissemination of information concerning its activities and the results thereof."
—NATIONAL AERONAUTICS AND SPACE ACT OF 1958

NASA SCIENTIFIC AND TECHNICAL PUBLICATIONS

TECHNICAL REPORTS: Scientific and technical information considered important, complete, and a lasting contribution to existing knowledge.

TECHNICAL NOTES: Information less broad in scope but nevertheless of importance as a contribution to existing knowledge.

TECHNICAL MEMORANDUMS: Information receiving limited distribution because of preliminary data, security classification, or other reasons. Also includes conference proceedings with either limited or unlimited distribution.

CONTRACTOR REPORTS: Scientific and technical information generated under a NASA contract or grant and considered an important contribution to existing knowledge.

TECHNICAL TRANSLATIONS: Information published in a foreign language considered to merit NASA distribution in English.

SPECIAL PUBLICATIONS: Information derived from or of value to NASA activities. Publications include final reports of major projects, monographs, data compilations, handbooks, sourcebooks, and special bibliographies.

TECHNOLOGY UTILIZATION PUBLICATIONS: Information on technology used by NASA that may be of particular interest in commercial and other non-aerospace applications. Publications include Tech Briefs, Technology Utilization Reports and Technology Surveys.

Details on the availability of these publications may be obtained from:

SCIENTIFIC AND TECHNICAL INFORMATION OFFICE

NATIONAL AERONAUTICS AND SPACE ADMINISTRATION
Washington, D.C. 20546